

2012

Implementation of Dual-Polarization on an Airborne Scatterometer and Preliminary Data Quality

Jason Dvorsky

University of Massachusetts Amherst

Follow this and additional works at: <https://scholarworks.umass.edu/theses>

 Part of the [Electromagnetics and Photonics Commons](#), [Signal Processing Commons](#), and the [Systems Engineering Commons](#)

Dvorsky, Jason, "Implementation of Dual-Polarization on an Airborne Scatterometer and Preliminary Data Quality" (2012). *Masters Theses 1911 - February 2014*. 743.

Retrieved from <https://scholarworks.umass.edu/theses/743>

This thesis is brought to you for free and open access by ScholarWorks@UMass Amherst. It has been accepted for inclusion in Masters Theses 1911 - February 2014 by an authorized administrator of ScholarWorks@UMass Amherst. For more information, please contact scholarworks@library.umass.edu.

**IMPLEMENTATION OF DUAL-POLARIZATION ON AN
AIRBORNE SCATTEROMETER AND PRELIMINARY
DATA QUALITY**

A Thesis Presented

by

JASON DVORSKY

Submitted to the Graduate School of the
University of Massachusetts Amherst in partial fulfillment
of the requirements for the degree of

MASTER OF SCIENCE IN ELECTRICAL AND COMPUTER ENGINEERING

February 2012

Electrical and Computer Engineering

**IMPLEMENTATION OF DUAL-POLARIZATION ON AN
AIRBORNE SCATTEROMETER AND PRELIMINARY
DATA QUALITY**

A Thesis Presented

by

JASON DVORSKY

Approved as to style and content by:

Stephen J. Frasier, Chair

Paul Siqueira, Member

Michael Zink, Member

Christopher V. Hollot, Department Chair
Electrical and Computer Engineering

ABSTRACT

IMPLEMENTATION OF DUAL-POLARIZATION ON AN AIRBORNE SCATTEROMETER AND PRELIMINARY DATA QUALITY

FEBRUARY 2012

JASON DVORSKY

B.Sc., UNIVERSITY OF MASSACHUSETT AMHERST

M.S.E.C.E., UNIVERSITY OF MASSACHUSETTS AMHERST

Directed by: Professor Stephen J. Frasier

The Imaging Wind and RAIN Profiler (IWRAP) is an airborne scatterometer system built and operated by University of Massachusetts Amherst's Microwave Remote Sensing Laboratory (MIRSL). The radar is seasonally deployed aboard one of the two National Oceanic and Atmospheric Administration (NOAA) WP-3D Orion "Hurricane Hunter" aircraft based out of MacDill AFB in Tampa, Florida. IWRAP is a dual-frequency, Ku- and C-band, scatterometer that uses two conically scanning antennas to estimate the ocean surface wind vectors as well as intervening rain profiles. Data that is gathered with IWRAP is used to improve current Geophysical Model Functions (GMF) or to help derive new GMFs for other undocumented incidence angles. This thesis outlines the improvements and changes made to the IWRAP system from 2009-2011. Chapter Two describes the IWRAP instrument including a description of the instrument status as of Fall 2009, and a summary of instrument operations in 2010 and 2011. Chapter Three describes hardware and software modifications to

support dual-polarization. It also describes hardware-based and flight-based attempts to observe at large incidence angles. Chapter Four is an analysis of the stability of the internal calibration both during flights and over a season. System documentation is consolidated into a single technical manual in Appendix A.

TABLE OF CONTENTS

| | Page |
|--|-------------|
| ABSTRACT | iii |
| LIST OF TABLES | vii |
| LIST OF FIGURES | viii |
| CHAPTER | |
| 1. INTRODUCTION | 1 |
| 1.1 Motivation | 1 |
| 1.2 Spaceborne Scatterometers | 3 |
| 1.3 Thesis Summary | 6 |
| 2. OVERVIEW OF IWRAP | 8 |
| 2.1 IWRAP Description as of Hurricane Storm 2009 | 8 |
| 2.2 Hurricane Storm Season 2010 Preparation and Deployment | 11 |
| 2.3 Winter Storm Season 2011 Preparation and Deployment | 12 |
| 3. HARDWARE AND SOFTWARE MODIFICATIONS | 14 |
| 3.1 Dual-Polarization | 14 |
| 3.1.1 Polarization Hardware Additions | 14 |
| 3.1.2 Polarization Signaling Additions | 16 |
| 3.2 Large Incidence Angles | 18 |
| 3.2.1 Circle Flight Measurements | 21 |
| 4. INTERNAL CALIBRATION STABILITY | 26 |
| 4.1 IWRAP Internal Calibration | 26 |
| 4.1.1 Hurricane Storm 2010 Season | 27 |

| | | |
|-----------|---|-----------|
| 4.1.1.1 | C-band | 28 |
| 4.1.1.2 | Ku-band | 29 |
| 4.1.2 | Winter Storm 2011 Season | 34 |
| 4.1.2.1 | C-band | 34 |
| 4.1.2.2 | Ku-band | 35 |
| 4.1.3 | Calibration stability summary | 38 |
| 4.2 | Encoder Signal Uncertainty | 41 |
| 5. | CONCLUSION | 44 |
| 5.1 | Summary of Work Completed | 44 |
| 5.2 | Future Work | 44 |
| | APPENDIX: IWRAP TECHNICAL MANUAL ADDITIONS | 46 |
| | BIBLIOGRAPHY | 56 |

LIST OF TABLES

| Table | Page |
|--|------|
| 2.1 Summary of HS2010 and WS2011 Storm Flights | 11 |
| 4.1 The standard deviation of the calibration pulse over the course of a season. The table includes all four channels for the HS2010 and WS2011 season. | 41 |

LIST OF FIGURES

| Figure | Page |
|--------|--|
| 1.1 | Example of geophysical model function at different wind speeds [8]. 2 |
| 1.2 | Global wind vector data obtained using SASS [3]. 4 |
| 1.3 | Characteristics of satellite scatterometers [9]. 6 |
| 2.1 | Department of Commerce WP-3D Orion “Hurricane Hunter” NOAA-43 9 |
| 2.2 | Graphic showing IWRAP’s two conically scanning beams [2]. 10 |
| 2.3 | Diagram showing the basic subsystems of Ku-band in single polarization mode. C-band has a similar structure [10]. 11 |
| 3.1 | These plots show mean NRCS for all frequency bands, polarizations and incidence angles versus wind speed in a log scale. This figure shows the saturation behavior of the mean NRCS. This behavior is less pronounced for C-band HH polarization at high incidence angles. The mean NRCS offset at 25 m/s is removed to normalize all curves to a common starting point [6]. 15 |
| 3.2 | (a) The C-band polarization switch mounted to the bottom of the antenna mount. (b) The C-band antenna mount with slip ring installed. 17 |
| 3.3 | The Ku-band front-end with the new polarization switch highlighted. 18 |
| 3.4 | Plot showing the difference in return power of the ocean surface between H- and V-polarizations. 19 |
| 3.5 | This plot shows antenna gain vs. incidence angle for the V-polarization patch on the Ku-band dual polarization antenna. The solid line is from measurements made by the manufacturer, Ball Aerospace Inc. The dotted line is an approximation of the gain past 50° of incidence. 21 |

| | | |
|------|---|----|
| 3.6 | Directivity vs. Scan Angle for the Ku-band dual polarization antenna. The H-polarized patch is being used for this measurement. Note that directivity drops off as scan angle increase toward 60° | 22 |
| 3.7 | A example of incidence angle versus azimuth beam look angle during a 10° circle flight pattern. The beam points to the front of the aircraft at an angle of 0° | 22 |
| 3.8 | The line represents the flight path taken during the winter storm flight on 01/23/11. The loops in the flight path represent circle patterns that were flown to obtain high incidence angle data. | 23 |
| 3.9 | Picture of the programmable synthesizer added to the C-band transceiver. This new addition allows the transmitted frequency to be changed during a flight. The Herley XS-5314 has a frequency range of 4.9 GHz to 5.5 GHz. | 24 |
| 3.10 | Picture of the programmable synthesizer added to the Ku-band transceiver. This new addition allows the transmitted frequency to be changed during a flight. The Herley XS-1437 has a frequency range of 12.2 GHz to 13.5 GHz. | 24 |
| 4.1 | This is the calibration pulse level from data taken from a flight on 8/28/10 through Tropical Storm Earl. Each point represents an average of the calibration pulse over a five minute period. | 27 |
| 4.2 | C-band Inner Angle Calibration Pulse Level for the 2010 hurricane season. The points represent the average pulse during a flight and the '±' represent the uncertainty of the average. The uncertainty is very small(i.e. negligible). | 28 |
| 4.3 | C-band Outer Angle Calibration Pulse Level for the 2010 hurricane season. The points represent the average pulse during a flight and the '±' represent the uncertainty of the average. The uncertainty is very small(i.e. negligible). | 29 |
| 4.4 | Ku-band Inner Angle Calibration Pulse Level for the 2010 hurricane season. The points represent the average pulse during a flight and the '±' represent the uncertainty of the average. The uncertainty is very small(i.e. negligible). | 31 |
| 4.5 | The Ku-band inner angle calibration pulse power versus antenna direction during a 2010 hurricane storm flight. Note that the power level changes with respect to the azimuth direction of the antenna. | 32 |

| | | |
|------|---|----|
| 4.6 | The Ku-band dual channel rotary joint's isolation between its two channels versus frequency. The isolation changes as the rotary joint turns. Figures 4.7 shows the isolation of the rotary joint when it has been rotated to a different azimuth angle than this plot. This helps show the change in isolation as the rotary joint turns. | 33 |
| 4.7 | The Ku-band dual channel rotary joint's isolation between its two channels versus frequency. The isolation changes as the rotary joint turns. Figures 4.6 shows the isolation of the rotary joint when it has been rotated to a different azimuth angle than this plot. This helps show the change in isolation as the rotary joint turns. | 33 |
| 4.8 | Ku-band Outer Angle Calibration Pulse Level for the 2010 hurricane season. The points represent the average pulse during a flight and the '±' represent the uncertainty of the average. The uncertainty is very small(i.e. negligible). | 34 |
| 4.9 | C-band Inner Angle Calibration Pulse Level for the 2011 winter season. The points represent the average pulse during a flight and the '±' represent the uncertainty of the average. The uncertainty is very small(i.e. negligible). | 36 |
| 4.10 | C-band Outer Angle Calibration Pulse Level for the 2011 winter season. The points represent the average pulse during a flight and the '±' represent the uncertainty of the average. The uncertainty is very small(i.e. negligible). | 37 |
| 4.11 | The highlighted component on the top of the diagram is the C-band power amplifier and the other component is the low noise amplifier. A lack of the necessary isolation between the devices has caused instability of the calibration pulse. | 38 |
| 4.12 | Ku-band Outer Angle Calibration Pulse Level for the 2011 winter season. The points represent the average pulse during a flight and the '±' represent the uncertainty of the average. The uncertainty is very small(i.e. negligible). | 39 |
| 4.13 | Ku-band Inner Angle Calibration Pulse Level for the 2011 winter season. The points represent the average pulse during a flight and the '±' represent the uncertainty of the average. The uncertainty is very small(i.e. negligible). | 40 |

| | | |
|------|--|----|
| 4.14 | The top plot shows the encoder position versus time from data taken during the 2010 hurricane season. The bottom plot shows the same encoder data versus data packets. Note that the drastic jump in encoder value does not appear when plotted versus time..... | 42 |
| 4.15 | Diagram illustrating the flow of the data stream inside the Pentek digital receiver. | 43 |
| A.1 | C-band RF and IF block diagram | 52 |
| A.2 | Ku-band RF and IF block diagram..... | 53 |
| A.3 | Picture of the box that houses the FPGA, DDS, and buffer boards. | 54 |
| A.4 | IWRAP's Altera Cyclone II FPGA used to generate control signaling for the radar | 54 |
| A.5 | IWRAP's buffer boards used to boost signaling from the FPGA to 5 volts | 55 |
| A.6 | A block diagram of IWRAP [10]. | 55 |

CHAPTER 1

INTRODUCTION

1.1 Motivation

Early radar operators observed background clutter on their radar displays when looking for sea vessels or airplanes over the ocean. This phenomenon was given the name sea clutter, which is caused by backscatter of microwave radar pulses from short capillary waves on the ocean surface. This sea clutter is what enables microwave scatterometers to measure the ocean surface wind vector. Scatterometers illuminate the wind-roughened ocean surface, and they measure the microwave backscatter. As the wind increases, so does the surface roughness and, in turn, the backscatter.

Airborne and spaceborne scatterometers commonly operate with incidence angles somewhere between 20 to 70 degrees to take advantage of Bragg scattering. Bragg scattering is the resonant interaction between the electromagnetic waves and the capillary waves on the sea surface. This occurs when the capillary waves' wavelength is one-half of the wavelength of the microwaves projected in the direction of the radar. When this condition is satisfied, the echoes from successive waves add in-phase. Bragg scattering will tend to dominate the return at these incidence angles. When the ocean surface is smooth, with little wind, there are no capillary waves and thus little or no return. When the wind increases, the surface will become rough with small waves which will cause constructive interference for centimeter wavelength microwaves, increasing the Normalized Radar Cross Section, or NRCS. This backscatter mainly depends on the magnitude of the wind but also to the wind direction as well. Equation (1.1) shows NRCS, represented as σ^o , and its relation to parameters from

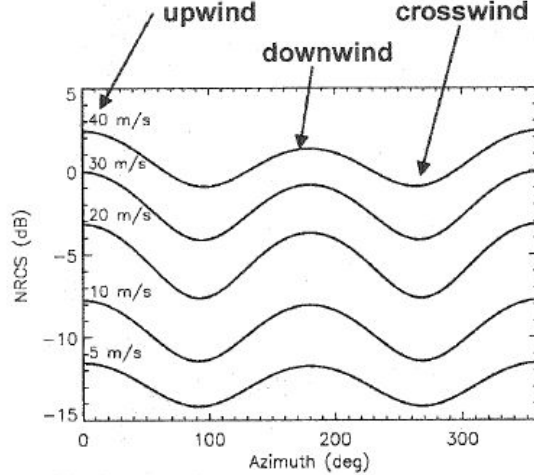


Figure 1.1: Example of geophysical model function at different wind speeds [8].

the radar range equation. The NRCS can be calculated using the parameter of the radar range equation using the following relation,

$$\sigma^o = \frac{(4\pi)^3 R^4 P_r}{P_t G^2 \lambda^2 A}, \quad (1.1)$$

where σ^o is the NRCS, R is the range to the target, P_r is the power received, P_t is the power transmitted, G is the antenna gain, λ is the wavelength of the transmitted waves, and A is the area illuminated.

Observing the ocean surface at different wind-relative azimuth angles enables scatterometers to measure the wind direction. The backscatter from the sea surface is modulated with respect to azimuth angle and cardinal directions can be referred to as upwind, crosswind or downwind as shown in Figure 1.1. This modulation of the return with respect to azimuth angle is commonly represented as a three-term Fourier series.

The NRCS can be converted into wind vectors using the *Geophysical Model Function* (GMF), which is an empirical relation between NRCS and the wind vector. Figure 1.1 shows a graphical example of NRCS vs. wind speed and direction. Theo-

retical studies of the relationship of backscatter from wind-roughened water has been tested in laboratories, and using the theory of Bragg scattering, various models have attempted to describe the returned signal. These idealized models have not proven accurate enough for wind retrievals on the open oceans. This is why the GMF is largely based on empirical fits of many radar observations to separately measured winds. Since it is a function of incidence angle, azimuth angle, frequency and polarization, the GMF varies between scatterometers with different specifications [14].

Severe hurricanes near the Americas, mid-latitude cyclones and typhoons in Asian waters are some of the most destructive of storms. In just the United States alone, hurricanes are responsible for at least 17,000 deaths since 1900 and hundreds of millions of dollars in damage every year. Information of the surface wind vectors inside these storms would be a very useful tool, as these measurements would help meteorologists to accurately identify gale-force winds of a storm. This will help provide the proper warning of flooding and high waves. Scatterometry radars are a very useful way to obtain such wind field data [4].

1.2 Spaceborne Scatterometers

Satellite scatterometers are a very useful tool for obtaining a large area of sea surface wind vectors. Once launched, their specifications are not changeable however, and because of their distance from their intended target, they have a poor spatial resolution. Since airborne scatterometers have lower altitudes they are able to obtain a much better range resolution and smaller azimuth resolution resulting in more detailed data. To create a GMF to relate NRCS to wind speed, data must be taken for a specific incidence angle, beam width and polarization. Using an airborne scatterometers is a good way to acquire data to create a GMF with different observing characteristics since these specifications can be easily modified [9].

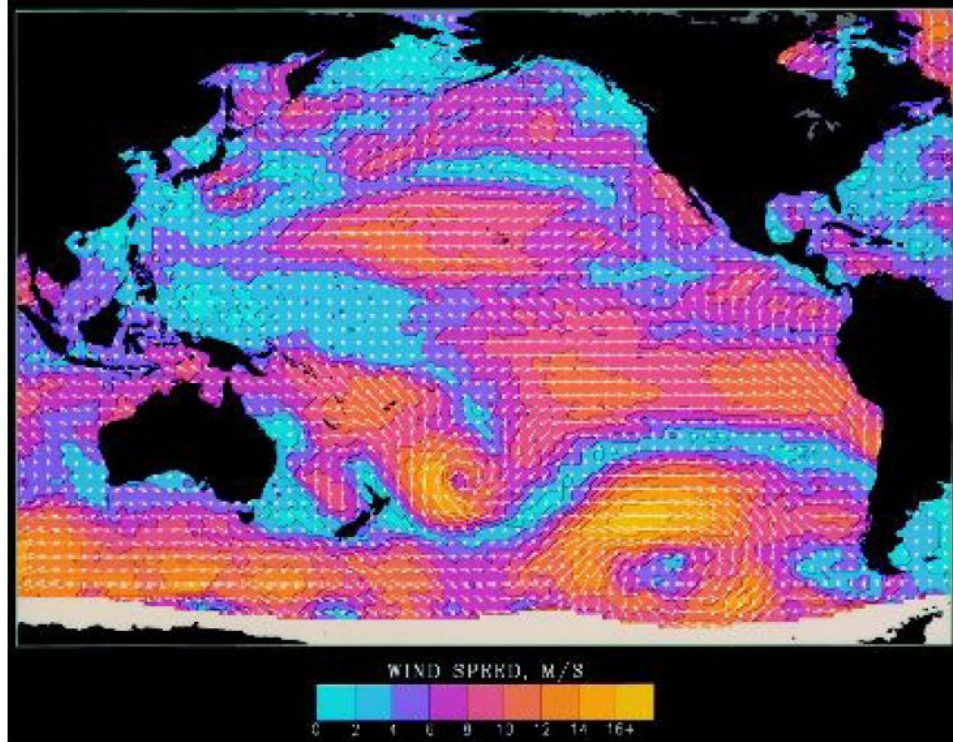


Figure 1.2: Global wind vector data obtained using SASS [3].

The first satellite scatterometer, RADSCAT, flew on board Skylab in 1973 to show the feasibility of space borne systems of that type. This was a prototype for the first satellite scatterometer called SeaSat-A Satellite Scatterometer (SASS) and provided the first accurate wind velocity vector measurements from space. Figure 1.2 shows global wind field data obtained using SASS. Seasat was launched in 1979 but only operated for 100 days before a catastrophic failure [5] [12].

The next satellite scatterometer to be launch was made by the European Space Agency (ESA) and was called ESCAT. It was on board ERS-1, launched on July 1991, and similar version on ERS-2 that launched in April 1995. This was a research satellite for testing the feasibility of different sensors, so its antennas were shared and only collected ocean surface wind vectors when in scatterometer mode. It operated at 5.3 GHz and had three fixed fan beams with incident angles from 18 to 59 degrees.

It had a single 500 km swath with a 25/50 km spatial resolution and roughly a 41 percent daily coverage. While the ERS-1 mission ended in March 2000, ERS-2 is still operational today [1].

The next satellite launched by the United States was NSCAT, on board the Japanese Aerospace Exploration's (JAXA) Advanced Earth Observing Satellite-I (ADEOS-I), which was launched August 1996. Its goal was to provide coverage every two days under all weather conditions. This was a similar design to SASS with 14 GHz center frequency and six fixed fan beam antennas. It had a 25/50 km resolution with two 300 km swaths and incident angles from 17 to 60 degrees. Unfortunately, a power failure terminated the mission earlier than expected in June 1997 [11].

To make up for the unfortunate loss of NSCAT, NASA launched an emergency recovery mission called SeaWinds. It was launched on board the QuikSCAT satellite in June 1999. A original version of SeaWinds was planned to be launch aboard JAXA's ADEOS-II at a later date along with other onboard remote sensing instruments. Sea-winds was a different design than previous satellite scatterometers. Instead of having fixed fan beam antennas it had a single azimuth scanning dish that created two pencil beams. It operated at 13.4 GHz and had an H-polarized inner beam at 46 degrees and a V-polarized outer beam at 54 degrees. The resolution was 25km/12.5 km with a 1400km/1800km swath and was able to achieve 92 percent coverage during a 24 hour period.

Since QuikSCAT's mission was a rush to fill the gap between the loss of NSCAT and the launch of ADEOS-II, it was not equipped with any other remote sensors. QuikSCAT lasted long past its expected life time and only recently stopped working in November 2009. A similar scatterometer to Seawind, called Seawinds-II, was launched on JAXA's ADEOS-II. It was launched on December 2002 but was short lived. In October 2003, ADEOS-II suffered a power failure and the mission was terminated. Figure 1.3 is a summary of the parameters of several past satellites [13].


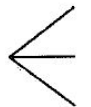
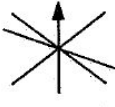

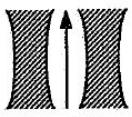

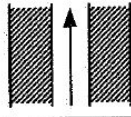
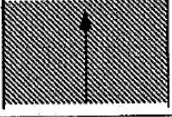
| | SEASAT | ERS-1/2 | NSCAT | QuikSCAT |
|-----------------|--|---|---|--|
| Frequency | 14.6 GHz | 5.3 GHz | 13.995 GHz | 13.402 GHz |
| Scan Pattern |  |  |  |  |
| Polarization | V-H, V-H | V ONLY | V, V-H, V | V, H |
| Inc. Angle | 22°-55° | 18°-47°, 24°-57° | 18°-57°, 22°-63° | 46°, 54° |
| Beam Resolution | Fixed Doppler | RANGE GATE | Variable Doppler | Spot |
| Resolution | 50 km | 50 km | 25 km | 25 km |
| Swath | 500 km 500 km  | 500 km  | 600 km 600 km  | 1800 km  |
| Daily Coverage | Variable | 41% | 77% | 93% |
| Dates | 6/78 – 10/78 | 8/91-1/01 | 8/96 – 6/97 | 6/99 + |

Figure 1.3: Characteristics of satellite scatterometers [9].

1.3 Thesis Summary

The Imaging Wind and RAIN Profiler (IWRAP) is an airborne scatterometer system built and operated by University of Massachusetts Amherst’s Microwave Remote Sensing Laboratory (MIRSL). The radar is seasonally deployed aboard one of the two National Oceanic and Atmospheric Administration (NOAA) WP-3D Orion “Hurricane Hunter” aircraft based out of MacDill AFB in Tampa, Florida. IWRAP is a dual-frequency, Ku- and C-band, scatterometer that uses two conically scanning antennas to estimate the surface wind vectors as well as intervening rain profiles. Data that is gathered with IWRAP is used to improve current GMF’s or to help derive new GMFs for other undocumented incidence angles.

This thesis outlines the improvements and changes made to the IWRAP system from 2009-2011. Chapter Two describes the IWRAP instrument including a description of the instrument status as of Fall 2009, and a summary of instrument operations in 2010 and 2011. Chapter Three describes hardware and software modifications to

support dual-polarization. It also describes hardware-based and flight-based attempts to observe at large incidence angles. Chapter Four is an analysis of the stability of the internal calibration both during flights and over a season. System documentation is consolidated into a single technical manual in Appendix A.

CHAPTER 2

OVERVIEW OF IWRAP

The Imaging Wind and RAin Profiler(IWRAP) is an airborne scatterometer system built and operated by the University of Massachusetts Amherst's Microwave Remote Sensing Laboratory(MIRSL). In partnership with NOAA's National Environmental Satellite, Data, and Information Service (NESDIS), MIRSL has been tasking IWRAP to obtain observations to aid in designing a future planned satellite scatterometer, the Dual Frequency Scatterometer (DFS). DFS has potential for a 50 percent improvement in accuracy of wind estimates in high wind regimes and a 20 percent improvement in resolution over QuikScat. It also will have the ability to observe through rain since it will employ both C-band as well as Ku-band radar systems. IWRAP is being used in a risk reduction effort that helps to understand the GMF at the specifications that are being considered for DFS. Changes have been made to the IWRAP system and data structure to be able to complete this objective. These changes, along with other modifications that have been made to IWRAP over the years, have been little documented. A new comprehensive overlook at the current state of the system is needed as well as a better understanding of the data quality.

[7]

2.1 IWRAP Description as of Hurricane Storm 2009

IWRAP is a high-resolution, dual-band, airborne radar that uses scatterometry to measure ocean surface winds. It also measures Doppler velocity and reflectivity profiles from intervening precipitation. The system is operated onboard the National



Figure 2.1: Department of Commerce WP-3D Orion “Hurricane Hunter” NOAA-43

Oceanic and Atmospheric Administration’s (NOAA) WP-3D aircraft as seen in Figure 2.1. This aircraft is specifically designed to operate in tropical cyclones. With its two conically scanning antennas, one Ku-band and the other C-band IWRAP scans the surface below the aircraft. Both antennas are microstrip patch arrays that transmit a pencil-beam that can be frequency-steered between 25 and 50 degrees incidence. The Ku-band antenna is a scaled-down version of the C-band antenna and because of this has similar beam characteristics.

At each frequency band, IWRAP transmits two pulses within each Pulse Repetition Interval (PRI). The center frequencies of the two pulses correspond to certain scan (incidence) angles. Typically, one of the incidence angles is fixed and is driven by an oven-controlled oscillator, while the other is driven by a programmable synthesizer that can be changed in frequency during flight by the radar operator. Since the pulses are transmitted nearly simultaneously, the down conversion and sampling

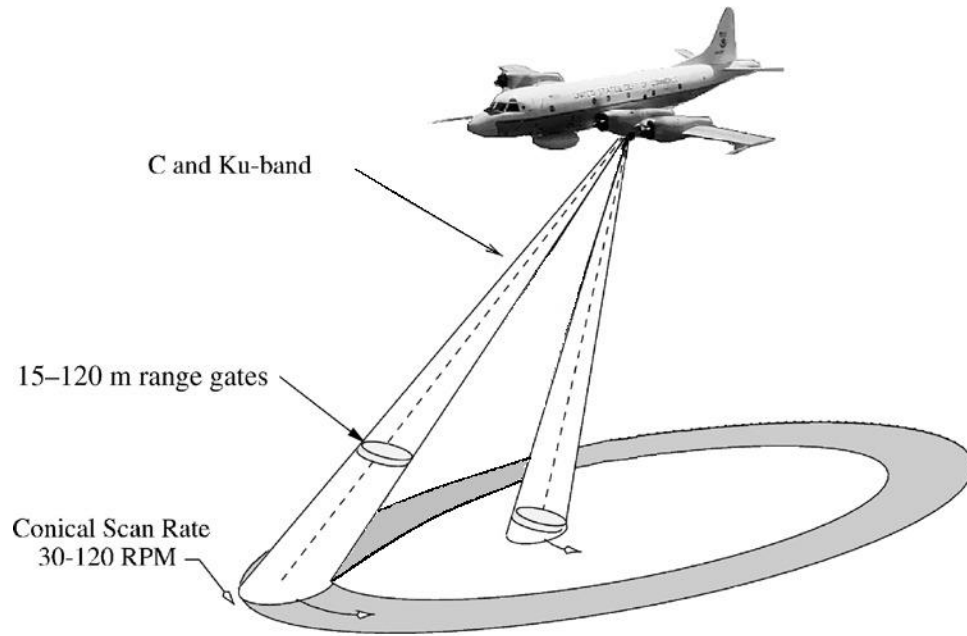


Figure 2.2: Graphic showing IWRAP's two conically scanning beams [2].

is done separately for each frequency. Figure 2.2 illustrate IWRAP's two conically scanning beams at different angles from its airborne platform [2].

Figure 2.3 shows the basic subsystems of the Ku-band system which has a very similar structure to the C-band radar. In the transceiver subsystem a 30 MHz pulse is generated by a Direct Digital Synthesizer(DDS) and is mixed to RF before it is amplified, filtered, and transmitted by the front-end. The front-end takes the signal and couples a portion of it to an internal calibration loop while the majority of the power is directed to the antenna. A transmit-receive switch before the antenna determines whether the radar will be in either transmit or receive mode. The returned signal enters the receiver chain which amplifies the echo signal using a Low Noise Amplifier (LNA). The signal is then split in the receiver, filtered depending on which frequency is desired, and then mixed with the 30 MHz intermediate frequency (IF) by the same oscillators used for up-conversion. Signals are then routed to the data acquisition

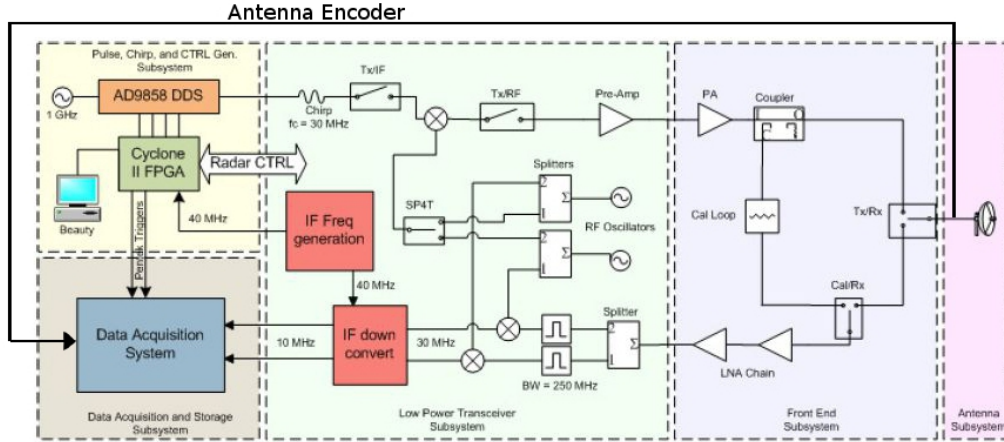


Figure 2.3: Diagram showing the basic subsystems of Ku-band in single polarization mode. C-band has a similar structure [10].

sub-system to be sampled and stored onto a RAID storage system. Navigation data, antenna position, and UTC time stamp are all saved along with the radar data.

2.2 Hurricane Storm Season 2010 Preparation and Deployment

Table 2.1: Summary of HS2010 and WS2011 Storm Flights

| Flight Summary | | | | |
|----------------|----------------|--------|------|--------------|
| 8/28 | T.S. Earl | T.S. | 1/13 | Winter Storm |
| 8/29 | Hurricane Earl | Cat. 1 | 1/17 | Winter Storm |
| 8/30 | Hurricane Earl | Cat. 4 | 1/23 | Winter Storm |
| 9/01 | Hurricane Earl | Cat. 4 | 1/24 | Winter Storm |
| 9/02 | Hurricane Earl | Cat. 4 | 1/25 | Winter Storm |
| 9/03 | Hurricane Earl | Cat. 4 | 1/30 | Winter Storm |
| 9/12 | AL92 | A.L. | 2/1 | Winter Storm |
| 9/13 | AL92 | A.L. | 2/7 | Winter Storm |

At the conclusion of the 2010 winter storm (WS2010) season, IWRAP was fully uninstalled from NOAA's WP-3D N43 aircraft. The radar was shipped back to

MIRSL to be modified and tested. The main goal was to outfit IWRAP so it would be able to collect data similar to the preliminary specifications of DFS. This was part of an ongoing effort to understand whether the specifications for DFS are optimal. One of the major changes to the system was the addition of dual-polarization capability. The other major change to the system was adding the ability to scan to large incidence angles. This will be discussed with more detail in Chapter Three.

IWRAP was reinstalled in July 2010 onto NOAA N43 to be ready for the upcoming hurricane season. During preparations for install, it was found that the Ku-band Microwave Power Module (MPM) amplifier was no longer working. This was replaced with a Ku-band Travelling Wave Tube Amplifier (TWTA). This new 250W Ku-band amplifier is much more powerful than the 70W MPM, but due to limitations of the front-end switching we did not use its full potential output power. The cabling for the high-power signal out of the Ku-band transmitter also broke at the connector during the install and was replaced. During this deployment, the Ku-band calibration pulse was observed to be unstable. This was due to an isolation problem and will be discussed in more detail in Chapter Four. The majority of the HS2010 flights were into Hurricane Earl, which was followed up the eastern seaboard. Two more flights were made into Atlantic Low 92 (AL92) from St. Croix. See Table 2.1 for the flight record for the HS2010 season.

2.3 Winter Storm Season 2011 Preparation and Deployment

Between the 2010 hurricane season and the winter storm (WS2011) season IWRAP remained installed on the NOAA P-3. The Ocean Winds winter storm project was then flown out of Halifax, Nova Scotia. We collected data during eight storm flights, and hurricane-force winds were observed in some of these. During some flights it was observed that the C-band calibration pulse was not stable, but this did not occur during ground testing. The problem was due to leakage from the C-band transmitter

directly into the calibration loop. The issue is discussed in more detail in Chapter Four. Table 2.1 gives a summary of all the flights made during the WS2011 season.

CHAPTER 3

HARDWARE AND SOFTWARE MODIFICATIONS

3.1 Dual-Polarization

Observing the ocean surface with different polarizations produce different observations. A GMF may have more desirable characteristics with a given polarization than the other. The model used to compare wind speed to NRCS begins to saturate as wind speed increases. This means that the NRCS increases less for higher wind speeds compared to low ones. This leads to greater error at high wind speed retrievals since a small deviation in the NRCS leads to a larger deviation in wind speed. It has been shown that this saturation is not as pronounced when using C-band frequencies, high incidence angles and a horizontally polarized beam. Figure 3.1 shows a comparison of this saturation with different frequencies, polarizations and incidence angles. If this result is correct, then high wind speed retrievals would be more accurate for horizontally polarized C-band measurements at larger incidence angles. IWRAP has been modified to collect dual-polarization data to better understand how the polarization affects the GMF as well as to give more versatility and value to these data [6].

3.1.1 Polarization Hardware Additions

The addition of dual-polarization to IWRAP required a number of changes. This required the addition of two new polarization switches, changes to the FPGA control signaling, a new polarization bit in the data stream, a slip-ring to supply signaling and changing to the dual polarization antennas. The polarization switches had to be

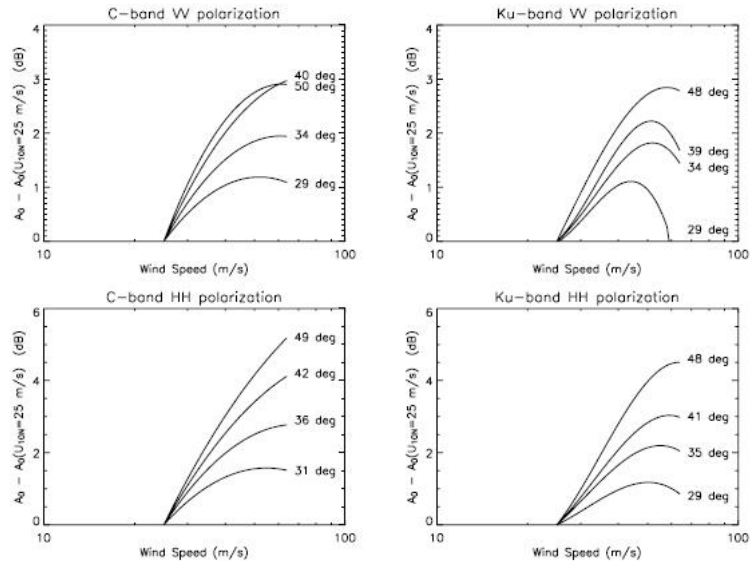


Figure 3.1: These plots show mean NRCS for all frequency bands, polarizations and incidence angles versus wind speed in a log scale. This figure shows the saturation behavior of the mean NRCS. This behavior is less pronounced for C-band HH polarization at high incidence angles. The mean NRCS offset at 25 m/s is removed to normalize all curves to a common starting point [6].

mounted to the antenna spinners for each radar. A Micronetics ES0012 is used as C-band radar's polarizations switch. The C-band rotary joint is now connected to the input of the ES0012 switch and the outputs are connected to the H-polarization and V-polarization ports of the antennas. Since the switch needs to spin with the antennas, a slip-ring was required to transport power and control signaling to the switch. A Fabricast 01-13578N slip-ring is used for this purpose. The C-band spinner mount can be seen in Figure 3.2. The Ku-band polarization switch is a Robinson Lab 2016-K148. A slip-ring was already a part of the Ku-band spinner assembly since the front-end was moved to the antenna for a better Signal to Noise Ratio (SNR) as described in [2]. The Ku-band polarization switch was added to the front-end box between the Transmit/Receive (TR) switch and the antennas. In preparation for the 2011 hurricane storm season, the Ku-band polarization switch was found to have too slow a switching speed to allow cross polarization measurements. This switch was removed and replaced by a Micronetics ES0013 which proved to be fast enough. Figure 3.3 shows the placement of the new Ku-band polarization switch.

3.1.2 Polarization Signaling Additions

The polarization switch is controlled by the Cyclone II FPGA to toggle back and forth between H- and V-polarization. The radar typically transmits 126 pulses in one polarization then switches to the other. The FPGA also provides a polarization switch status bit that is included in the data stream. This value is added to the most significant bit of the long integer 'status' which is one of the variables from IWRAP's raw data structure. During the 2010 hurricane season the polarization status signal was wired from the FPGA to a digital I/O pin on a data acquisition card built by Pentek. Data acquisition software was modified to read the digital value with each block of radar data. However, reading the digital I/O had the undesired effect of dropping the data rate in half. The time required to read the digital I/O caused the

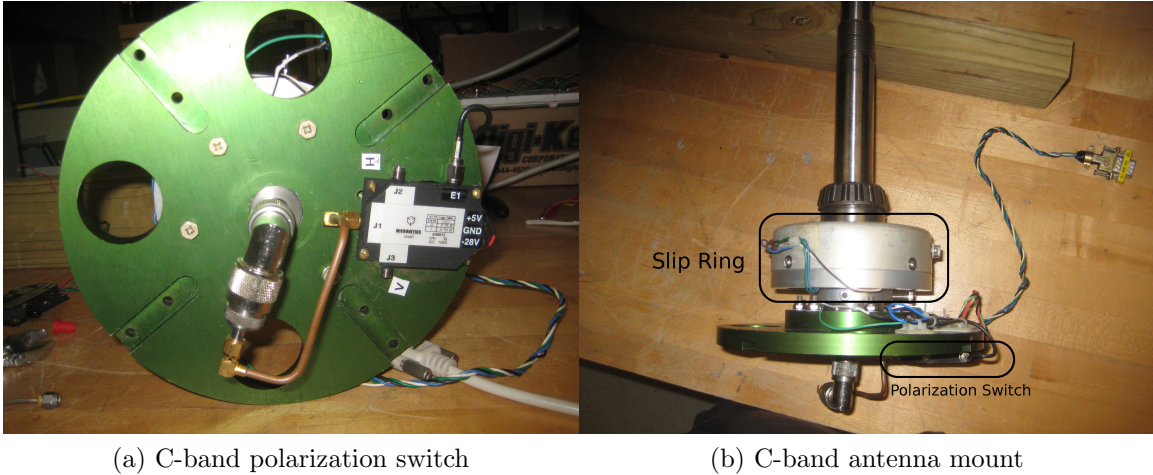


Figure 3.2: (a) The C-band polarization switch mounted to the bottom of the antenna mount. (b) The C-band antenna mount with slip ring installed.

acquisition software to miss alternate packets of data. Thus, in preparation for the 2011 winter storm season the polarization status signal was removed from the Pentek data acquisition card and moved to an extra bit in the antenna encoder position data stream.

The polarization switch status and the antenna encoder position are merged with the raw inphase and quadrature radar data with acquisition code that is running while the system is operating. The acquisition code can come out of synchronization when combining the raw I and Q data with the rest of the data stream (time stamp, antenna encoder, etc.). This can cause the polarization status being saved incorrectly, where H-polarized data is being saved as V-polarized data and vice versa. This problem would happen around the edges of the transition between polarizations. This can be fixed in post processing by comparing the return echoes from the surface. The V-polarized surface echo is roughly 5 dB higher than H-polarized returns. By comparing the return power, the synchronization errors of the polarization switch state can be corrected. Figure 3.4 shows the difference in the power returned from the surface between H- and V-polarized IWRAP data (the cause of this synchronization issue is

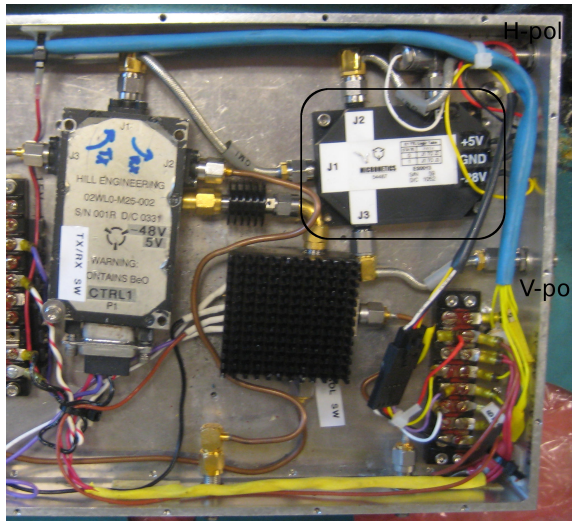


Figure 3.3: The Ku-band front-end with the new polarization switch highlighted.

discussed in more detail in Chapter Four). This figure shows power vs. range, as measured by the Pentek data acquisition card. The left-most peak is the calibration pulse is a sample of the transmitted pulse. Matched filtering was applied to improve range resolution and to achieve a good SNR. The next peak is the nadir echo which is the return from the antenna beam's sidelobes followed by the surface echo. This is where the difference between polarization returns can be seen. The V-polarized return is noticeably higher than H-polarized return. The time difference between the H- and V-polarized plots in Figure 3.4 is less than 10 milliseconds, hence it is expected that the sea surface state is the same for both data sets.

3.2 Large Incidence Angles

The National Oceanic and Atmospheric Administration (NOAA) is in the early phases of determining the specifications for a new satellite based scatterometer to replace the defunct Quikscat. A possible deployment platform would require the incidence angle to be approximately 60° where a GMF is as yet undefined. This is

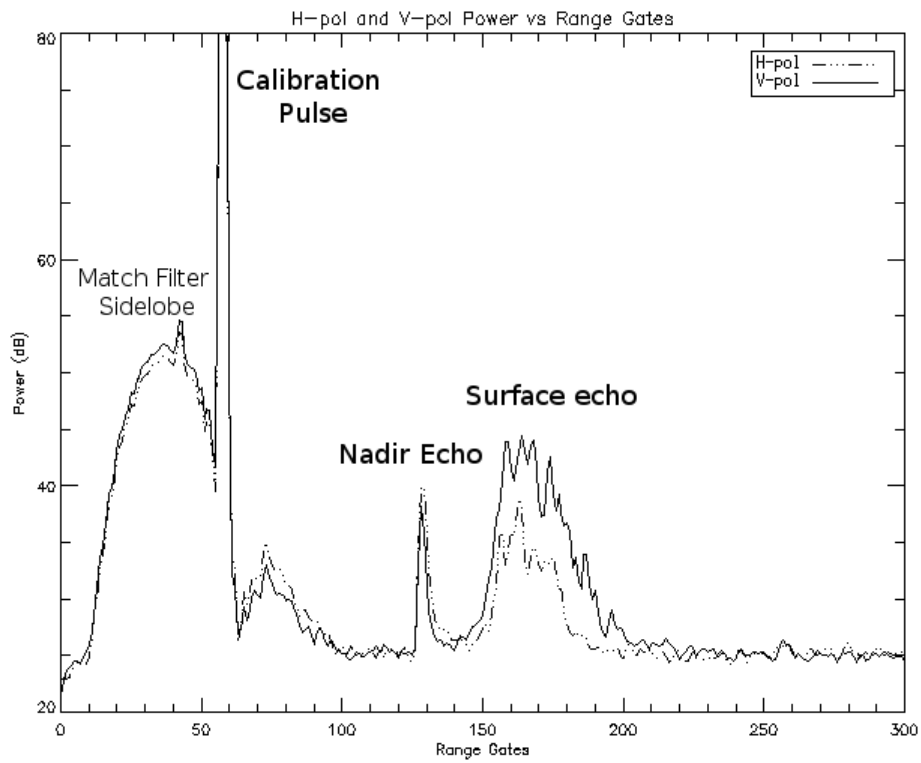


Figure 3.4: Plot showing the difference in return power of the ocean surface between H- and V-polarizations.

due to restriction of the proposed satellite's orbit. IWRAP was called upon to collect data at new incidence angles to understand if they are a viable design specification.

Incidence angles greater than 50° are beyond IWRAP's standard range, and the system lacked ability to change frequency easily during a flight experiment. To improve this, the oscillator for one of the two channels for each frequency band was replaced with an RF synthesizer. These synthesizers were rack-mounted instruments and were manually set to the proper settings. This helped to determine which transmission frequency would result in an incidence angle of 60° since the relationship between frequency and scan angle is unknown past 50° .

Measurements were attempted in storms during the 2010 hurricane season at 60° but obtaining reasonable data turned out to be not viable. The antennas were made to be optimal at a 30° scan angle and were not designed to work at 60° . As the scan angle increases toward 60° the gain decreases and the beamwidth becomes wider reducing the overall power returned from the ocean surface. This can be seen in Figure 3.5, which shows the gain vs. incidence angle for the Ku-band antenna. In addition to the loss of ideal antenna parameters, increasing the antenna's scan angle increases the path the transmitted waveform travels which add to the general reduction to returned power from these measurements.

Using the UMass near-field antenna range, measurements were made of the Ku-band antenna to better understand the antenna patterns for these higher scan angles. These measurements were expected to be analogous to the C-band's antenna since the Ku-band antenna is a scaled version of that design. Figure 3.6 shows the Ku-band H-polarized antenna's elevation pattern measured scan angles from 35° to 60° . The directivity drops roughly 3 dB from 50° scan angle up to 60° . This will cause an overall drop of 6 dB of the radar's SNR just from loss of gain alone.

More troubling were differences in the measured patterns from the data provided by the manufacturer. These may have been caused by imperfections in the test range

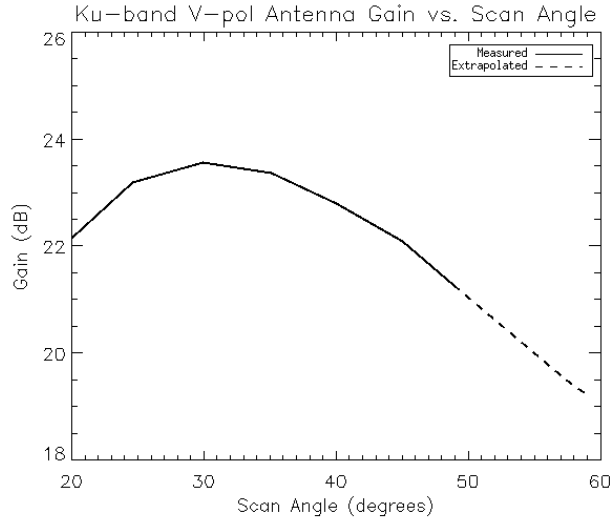


Figure 3.5: This plot shows antenna gain vs. incidence angle for the V-polarization patch on the Ku-band dual polarization antenna. The solid line is from measurements made by the manufacturer, Ball Aerospace Inc. The dotted line is an approximation of the gain past 50° of incidence.

(reflections from the floor). The inability to reproduce “known” measurements cast doubt on our ability to determine the absolute gain of the antenna. Because of these limitations, it was necessary to explore different ways to collect higher incidence angle measurements.

3.2.1 Circle Flight Measurements

Another way to observe at large incidence angle is to record data while the plane is flying in a circle pattern with a constant roll angle. With this flight path, the conically-scanning beam impinging on the ocean surface will trace out an ellipse with incidence angles varying depending on the azimuthal look direction. The incidence angle upon the surface is calculated by taking the nominal incidence angle plus or minus the aircraft’s roll angle. When the beam is pointing fore or aft of the aircraft the nominal incidence angle is measured. Figure 3.7 is an example of incidence angle vs. azimuth scan angle during a circle flight. This allowed measurements to be taken

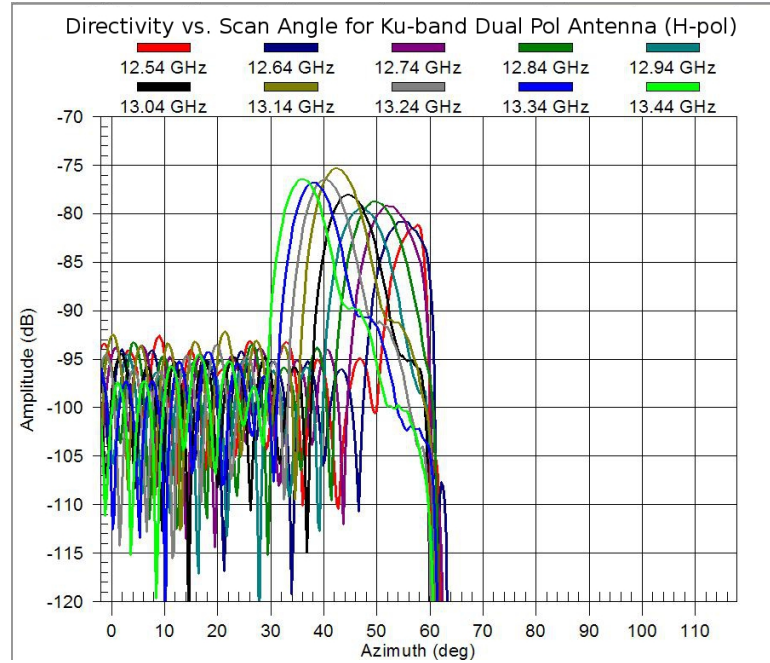


Figure 3.6: Directivity vs. Scan Angle for the Ku-band dual polarization antenna. The H-polarized patch is being used for this measurement. Note that directivity drops off as scan angle increase toward 60° .

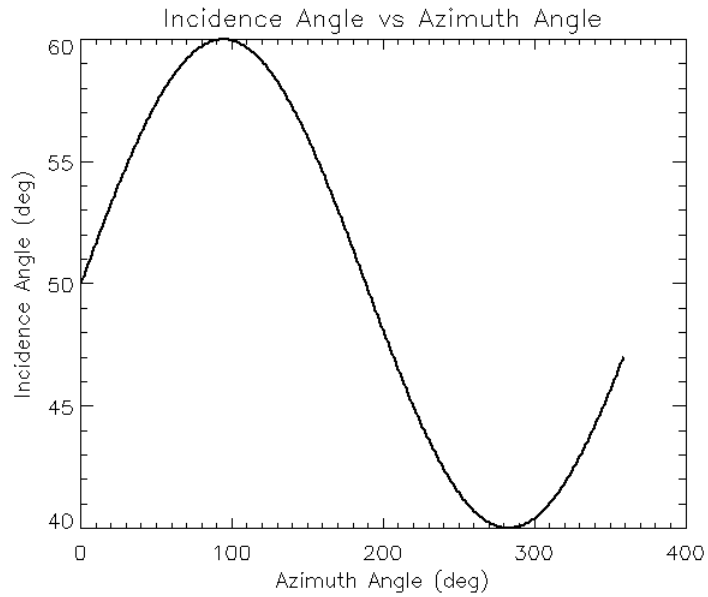


Figure 3.7: A example of incidence angle versus azimuth beam look angle during a 10° circle flight pattern. The beam points to the front of the aircraft at an angle of 0° .

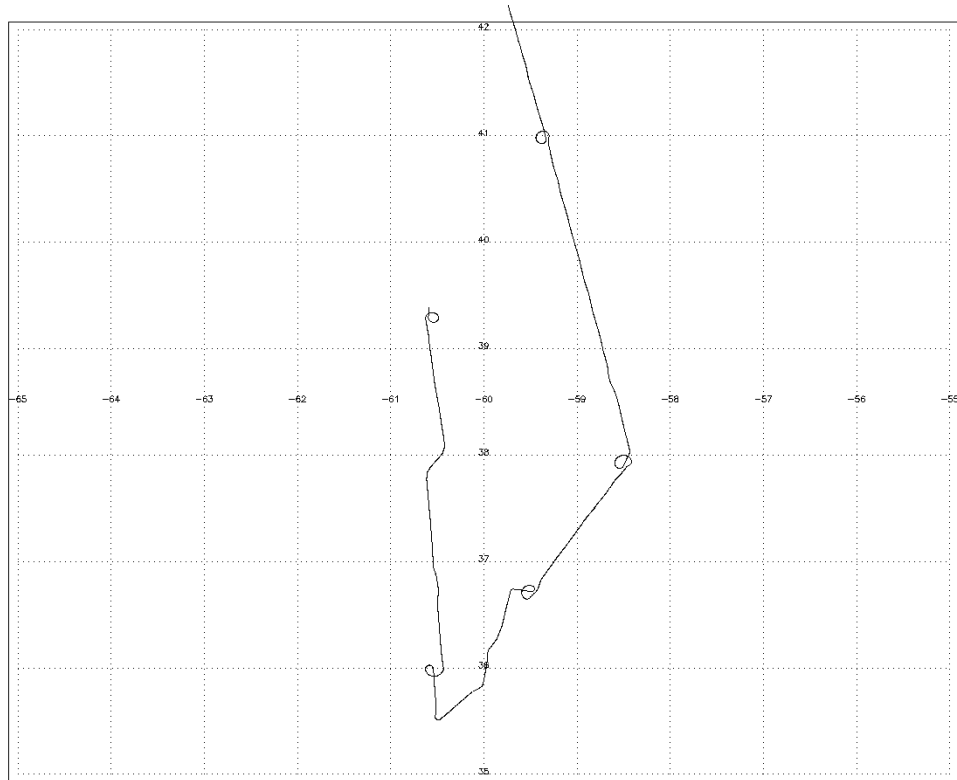


Figure 3.8: The line represents the flight path taken during the winter storm flight on 01/23/11. The loops in the flight path represent circle patterns that were flown to obtain high incidence angle data.

with incidence angles between 20° to 60° . A drawback of this measurement setup is that the Step Frequency Microwave Radiometer (SFMR) that provides independent measurements of the wind speed, does not work correctly when the aircraft is in a circle pattern as it is designed for nadir-looking operation. The SFMR measurements before and after a circle flight must be used as the wind speed reference for IWRAP data taken during a circle pattern. This has proven to be an effective way to measure a broad range of incidence angles. Figure 3.8 shows the aircraft's flight path when circle flights were performed.

During the pre-season work for the 2011 winter storm season, compact synthesizers were added into the Ku-band and C-band transceivers replacing the external rackmount synthesizers used previously. These new devices allow for a change in

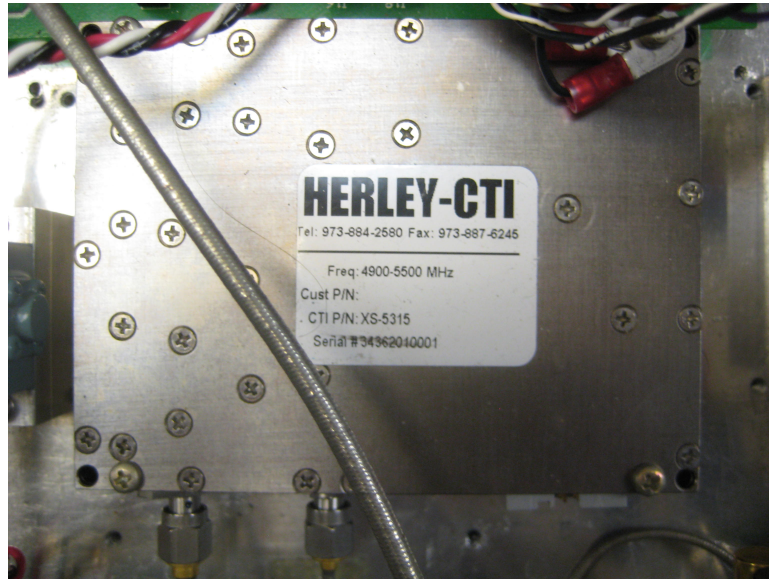


Figure 3.9: Picture of the programmable synthesizer added to the C-band transceiver. This new addition allows the transmitted frequency to be changed during a flight. The Herley XS-5314 has a frequency range of 4.9 GHz to 5.5 GHz.



Figure 3.10: Picture of the programmable synthesizer added to the Ku-band transceiver. This new addition allows the transmitted frequency to be changed during a flight. The Herley XS-1437 has a frequency range of 12.2 GHz to 13.5 GHz.

transmitted frequency for the outer incidence angle for each radar. This frequency can be changed by the radar operator during a storm flight using the IWRAP Graphical User Interface (GUI). These synthesizers were placed in the transceivers in place of one of the RF oscillators. Appropriate wiring was included between the transceiver and the FPGA so the synthesizers could be programmed by the FPGA. The new synthesizers can be seen in Figure 3.9 and Figure 3.10.

CHAPTER 4

INTERNAL CALIBRATION STABILITY

This chapter discusses the integrity of the radar data taken during the 2010 hurricane storm season (HS2010) and 2011 winter storm season (HS2011). It includes a description of the two deployments, as well a discussion of the stability of IWRAP's internal calibration pulse and synchronization issues that were encountered.

4.1 IWRAP Internal Calibration

When IWRAP transmits, a portion of the transmitted signal is coupled off and attenuated so it may be sampled and saved to disk along with the echo signal. This is called the calibration pulse. Recording the calibration pulse provides a record of how much power was transmitted. Without knowledge of the transmitted power the NRCS could not be calculated precisely. This section examines the stability of the calibration pulse from the past two seasons. Plots of calibration pulse that are presented in this section have been adjusted to remove known changes to the system operation or changes to attenuation that the calibration signal experiences. For example, the use of pulse compression will change the amplitude of the calibration pulse. This is done so that unknown variations are easier to identify and to quantify.

Figure 4.1 shows the calibration pulse during the course of a storm flight into Tropical Storm Earl on 08/28/10. Each point represents an average of the calibration pulse over a five minute period. The power level reduces for the first half hour but then remains nearly constant for the remainder of the flight. These changes are attributed to the change in operating temperature of the system as it warms up. Overall the

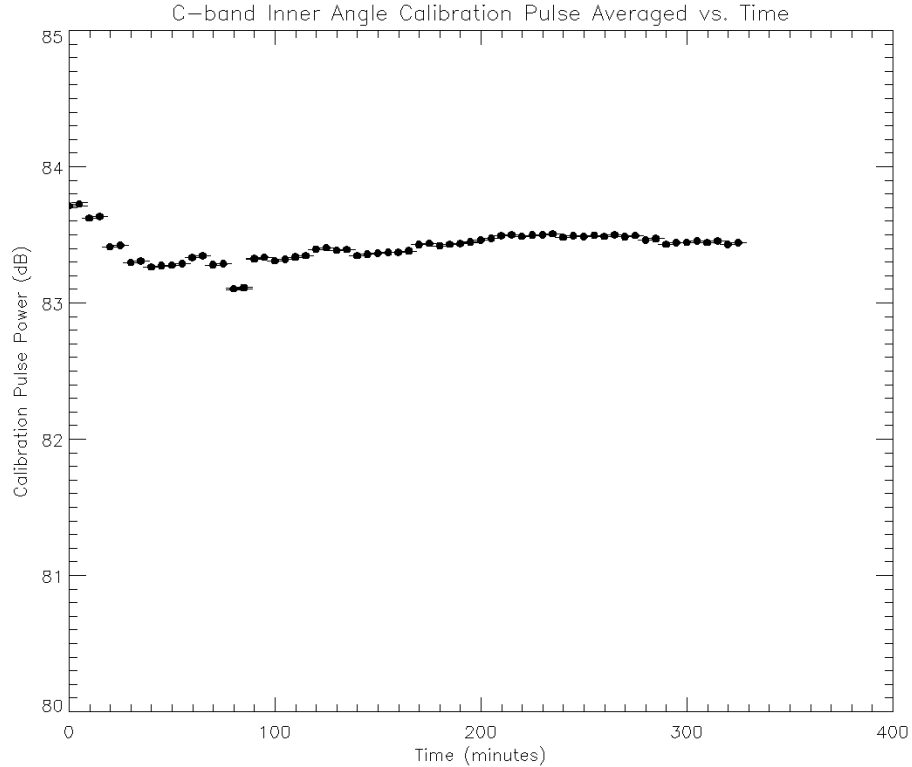


Figure 4.1: This is the calibration pulse level from data taken from a flight on 8/28/10 through Tropical Storm Earl. Each point represents an average of the calibration pulse over a five minute period.

level remains fairly constant with a average calibration pulse level of 83.414 dB and a standard deviation 0.357 dB. The units are digital counts expressed in dB.

4.1.1 Hurricane Storm 2010 Season

The two channels of each frequency band were swapped between 8/30 and 9/01 of the HS2010 season. The channel that is transmitted first, Channel One, is connected to the RF synthesizer at the time of this writing. This channel generally transmits at larger incidence angles. Channel Two is used for the inner incidence angle. This was done so that a longer chirp pulse could be transmitted for the larger incidence angle channel to increase the SNR. This need for an increase in signal return was required since a larger than normal incidence angle was being used. However, in addition,

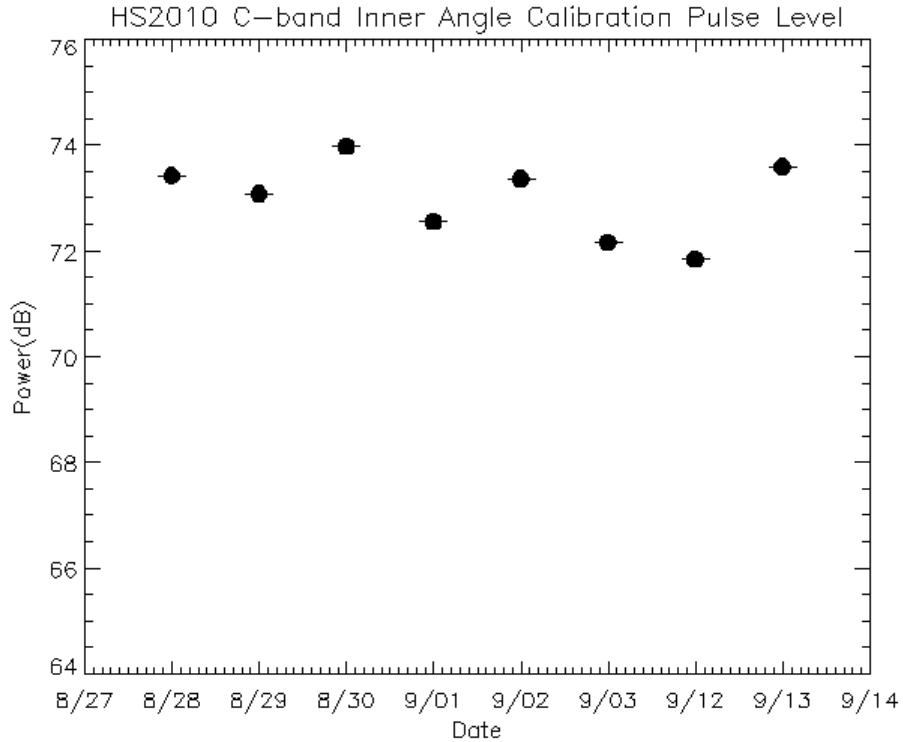


Figure 4.2: C-band Inner Angle Calibration Pulse Level for the 2010 hurricane season. The points represent the average pulse during a flight and the '-' represent the uncertainty of the average. The uncertainty is very small (i.e. negligible).

several flights were carried out at higher altitudes than usual requiring additional pulse compression gain to obtain a reasonable SNR.

4.1.1.1 C-band

Figure 4.2 shows the calibration pulse level of the C-band inner angle for HS2010. The fluctuations in power may be caused by the sampling card not sampling the peak at all times. When restarting the system, the peak power may be slightly different than previously observed using all of the same settings. Extending the length of a pulse reduces this effect. Another cause of changes from day-to-day are fluctuations of the system temperature. The average power for the calibration pulse for this channel is 72.992 dB for the season with a standard deviation of 0.742 dB

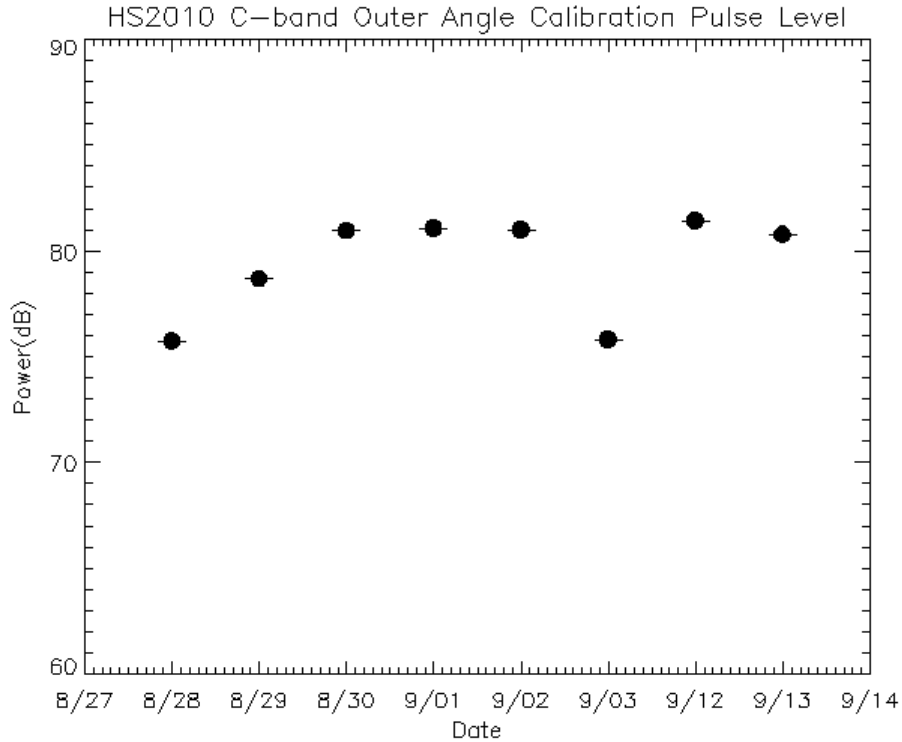


Figure 4.3: C-band Outer Angle Calibration Pulse Level for the 2010 hurricane season. The points represent the average pulse during a flight and the '-' represent the uncertainty of the average. The uncertainty is very small (i.e. negligible).

Figure 4.3 shows the calibration pulse level of the C-band outer angle for HS2010. There are fluctuations from day-to-day for this channel. This channel shows a fair amount of fluctuation from day to day. This may be caused by the finite isolation that is seen in the C-band front-end during WS2011. This isolation problem is discussed in greater detail in section 5.1.2.1. This also could be the caused be a loose connection that only this channel experiences. The average calibration pulse for this channel for the season is 79.4291 dB with a standard deviation of 2.4092 dB

4.1.1.2 Ku-band

Figure 4.4 shows the calibration pulse level of the Ku-band inner angle for HS2010. It was observed that Ku-band's calibration pulse would fluctuate while the antenna's

were spinning. Figure 4.5 shows this fluctuation of the calibration pulse power with respect to the antenna look direction. The plot shows that the power level varies as much as 10 dB at times depending on the antenna look direction. It was determined that this variation is caused by the finite, and inadequate, isolation of the dual-channel rotary joint. The rotary joint supplies signal back and forth to the spinning antennas. One channel of the rotary joint carries the transmit pulse while the other carries return signal to the receiver. During transmission some signal leaks from the transmit channel of the rotary joint directly to the receive channel. Since the calibration signal attenuated by the calibration loop is weaker than the transmit signal, the leakage from the transmit channel overpowers it. The cause of this fluctuation with respect to the antenna look direction is the result of the rotary joint isolation's dependence on the rotation angle. Figures 4.6 and 4.7 show plots of the rotary joint's isolation. The rotation angle is 90 degrees different between the plots, which shows a change in isolation by roughly 9 dB. The reason this was not observed in previous deployments is that a different Ku-band LNA is being used to amplify the calibration signal before it reaches the rotary joint. The prior LNA, which had more gain, broke just prior to the HS2010 season and was sent out for repair. The broken LNA had a gain of 48.7 dB at 13.5 GHz while the replacement had an average gain of 43.73 dB at that frequency. The replacement LNA did not amplify the calibration signal sufficiently to overcome the finite isolation of the rotary joint. In post processing, a measured value for the power transmitted was used to override the value based off the calibration pulse. The average calibration pulse for the Ku-band inner channel for the season is 82.1875 dB and the standard deviation is 10.245 dB.

Figure 4.8 shows the calibration pulse level of the Ku-band outer angle for HS2010. The isolation issue with the rotary joints has caused fluctuations in the calibration power level but to a lesser extent. This is because the transmitted frequency for the outer angle, 12.89 GHz, generally exhibits greater rotary joint isolation than the

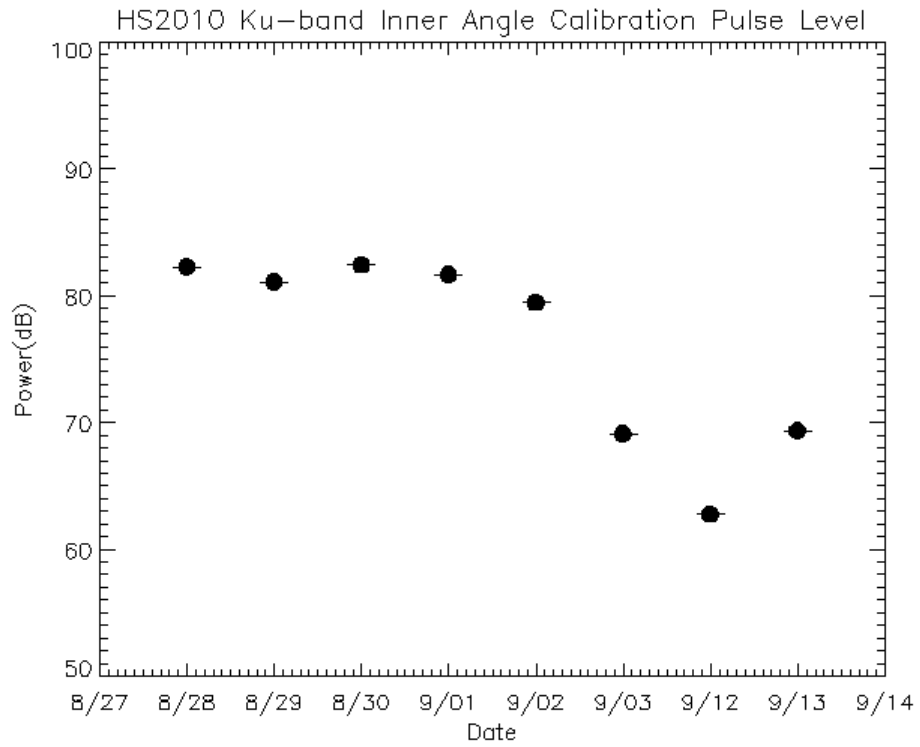


Figure 4.4: Ku-band Inner Angle Calibration Pulse Level for the 2010 hurricane season. The points represent the average pulse during a flight and the '-' represent the uncertainty of the average. The uncertainty is very small(i.e. negligible).

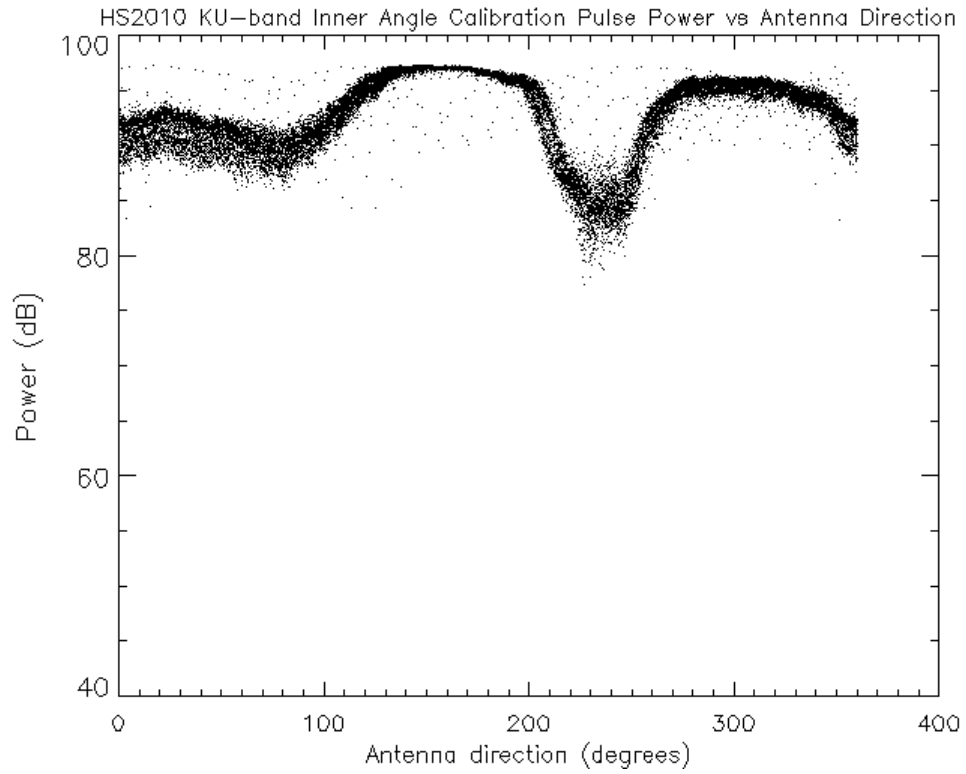


Figure 4.5: The Ku-band inner angle calibration pulse power versus antenna direction during a 2010 hurricane storm flight. Note that the power level changes with respect to the azimuth direction of the antenna.

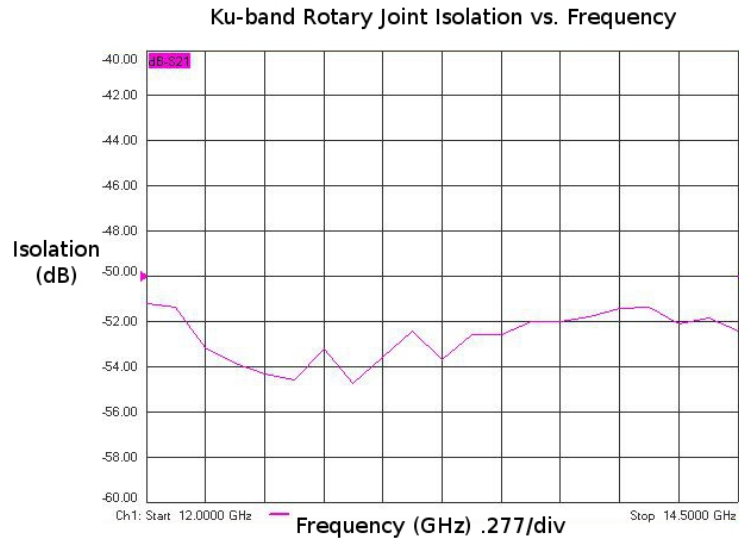


Figure 4.6: The Ku-band dual channel rotary joint’s isolation between its two channels versus frequency. The isolation changes as the rotary joint turns. Figures 4.7 shows the isolation of the rotary joint when it has been rotated to a different azimuth angle than this plot. This helps show the change in isolation as the rotary joint turns.

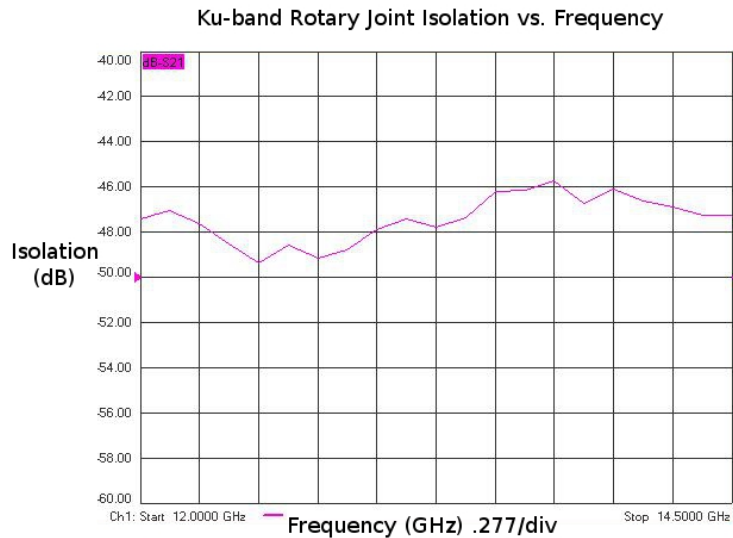


Figure 4.7: The Ku-band dual channel rotary joint’s isolation between its two channels versus frequency. The isolation changes as the rotary joint turns. Figures 4.6 shows the isolation of the rotary joint when it has been rotated to a different azimuth angle than this plot. This helps show the change in isolation as the rotary joint turns.

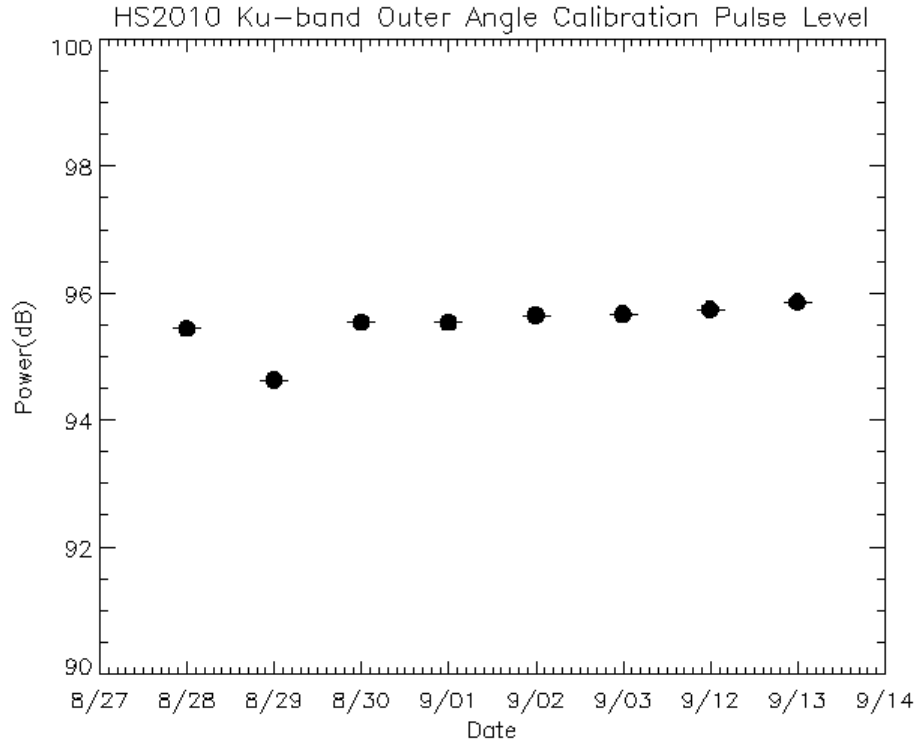


Figure 4.8: Ku-band Outer Angle Calibration Pulse Level for the 2010 hurricane season. The points represent the average pulse during a flight and the '-' represent the uncertainty of the average. The uncertainty is very small(i.e. negligible).

inner angle frequency of 13.5 GHz. This can be seen in Figures 4.6 and 4.7. The average calibration pulse for Ku-band outer channel for the season is 95.51 dB and the standard deviation is 0.377 dB

4.1.2 Winter Storm 2011 Season

4.1.2.1 C-band

Figure 4.9 and Figure 4.10 show the calibration pulse level of the C-band WS2011, outer and inner angle respectively. Both of these channels also showed a fluctuating calibration pulse during storm flights. This behavior would not occur while the plane was on the ground which made the problem difficult to find. During the Winter 2011 deployment, it was discovered that the cause of the fluctuation was leakage from

the C-band power amplifier output to the LNA. Figure 5.11 highlights the amplifier and the LNA. These components seem far away in the diagram but are actually within close proximity in the C-band front-end. This leakage was occurring through the air from one cable to the other. This leakage was overpowering the calibration signal that is amplified by the LNA. The reason this problem only occurred during flight was because in-flight turbulence would cause the metal lid of the box housing these components to vibrate. It is believed that this vibration of the lid changed the environmental effect of the leakage had on the LNA.

It was necessary to either improve the isolation between the components or to strengthen the calibration signal. This was done in the field by removing some of the attenuation that the calibration signal experiences. A total of 20 dB of attenuation was removed from the C-band calibration loop, which reduced fluctuations to less than 1 dB. This change was made prior to the flight on 2/01/11. The total calibration loop attenuation was originally 102 dB before the change and is now 82 dB. After the change was made the calibration pulse power proved to be stable. Removing attenuation from the calibration loop increased the signal level beyond the range of the Pentek digital receiver card, so attenuation was added just prior to its input. Channel One received 7 dB of attenuation and Channel Two received 9 dB. The average calibration pulse for the C-band inner channel for the season is 80.535 dB and the standard deviation is 3.091 dB. The average calibration pulse for C-band outer channel for the season is 93.4156 dB and the standard deviation is 4.641 dB.

4.1.2.2 Ku-band

Figure 4.12 shows the calibration pulse level of the Ku-band outer angle for WS2011. The broken LNA, a Miteq AMF-6F-12001800-13-10P, was fixed and re-installed for this WS2011 season. This LNA has more gain so the leakage between rotary joint channels was no longer a problem. The calibration pulse level was very

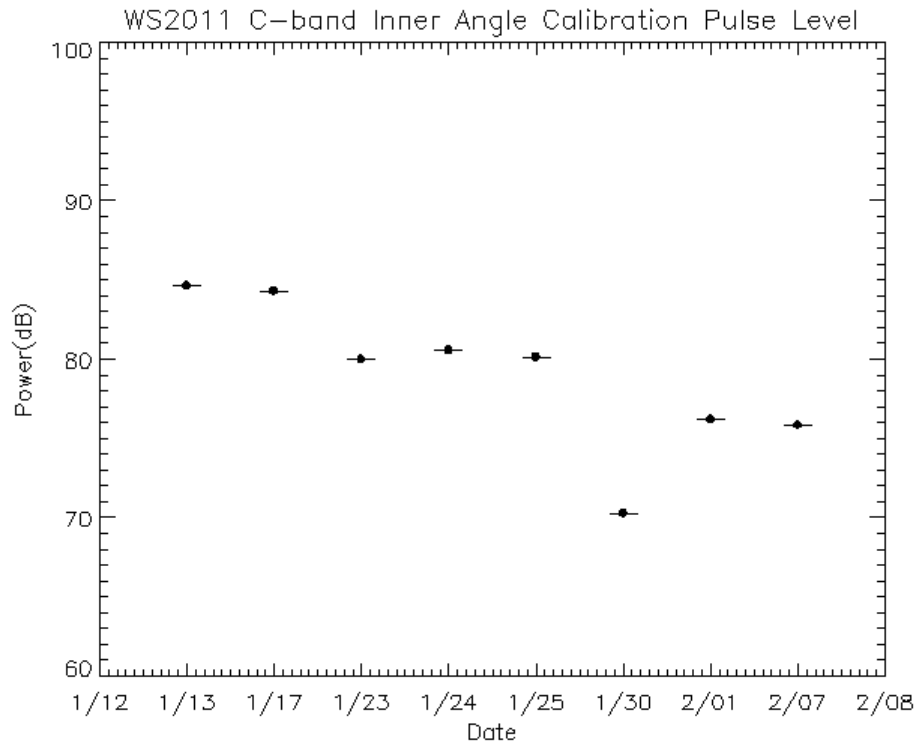


Figure 4.9: C-band Inner Angle Calibration Pulse Level for the 2011 winter season. The points represent the average pulse during a flight and the '-' represent the uncertainty of the average. The uncertainty is very small(i.e. negligible).

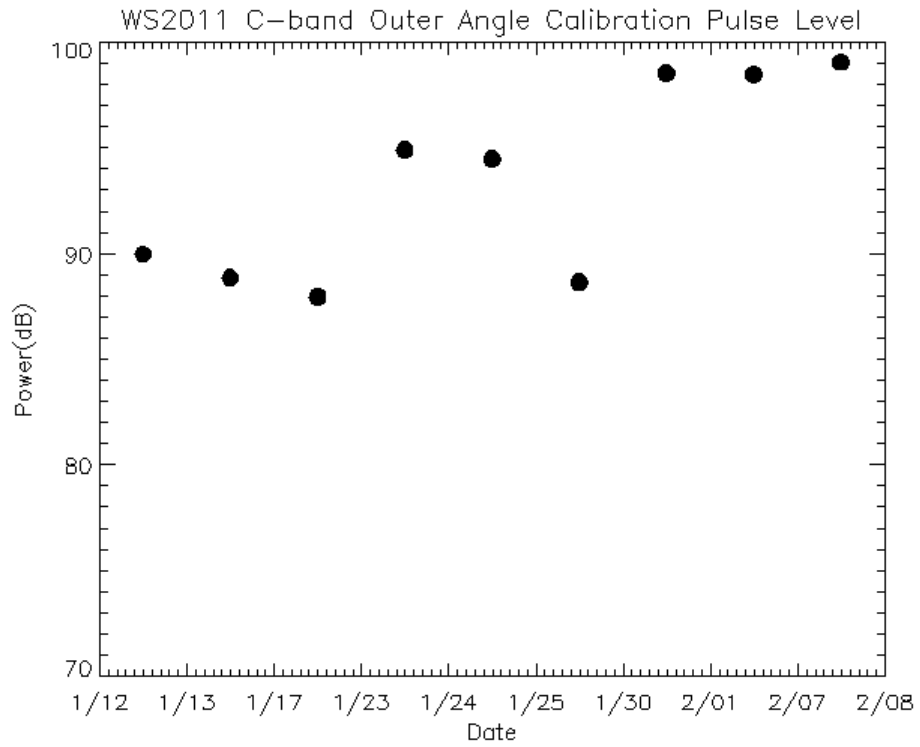


Figure 4.10: C-band Outer Angle Calibration Pulse Level for the 2011 winter season. The points represent the average pulse during a flight and the '-' represent the uncertainty of the average. The uncertainty is very small(i.e. negligible).

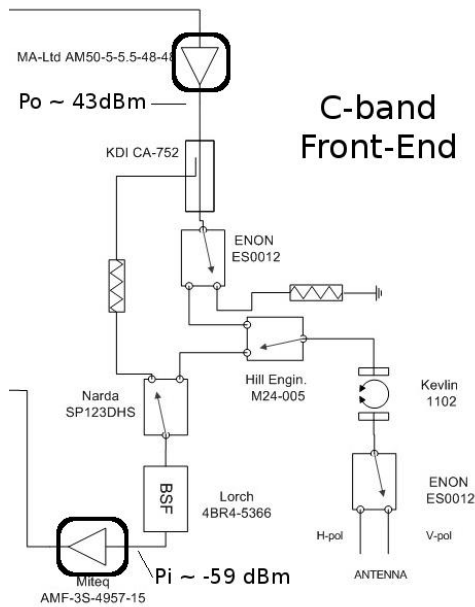


Figure 4.11: The highlighted component on the top of the diagram is the C-band power amplifier and the other component is the low noise amplifier. A lack of the necessary isolation between the devices has caused instability of the calibration pulse.

stable throughout the season. The average calibration pulse for Ku-band outer channel for the season was 96.6057 dB and the standard deviation was 0.4015 dB.

Figure 4.13 shows the calibration pulse level of the Ku-band inner angle. The reason for the drop in power level during the flight on 2/07/11 is unknown. The noise level dropped as well. This problem occurred part way through a flight. Hence, it is suspected that a loose connection somewhere in the transceiver or in the cabling between the receiver and the data acquisition card is the cause. Data from this data collection was not considered when calculating the mean and standard deviation for the calibration pulse for the season. The average calibration pulse for Ku-band inner channel for the season is 85.565 dB and the standard deviation is 0.545 dB.

4.1.3 Calibration stability summary

Table 4.1 shows the standard deviation of the calibration pulses for all four channels during the HS2010 and WS2011 seasons. Overall, IWRAP's internal calibration

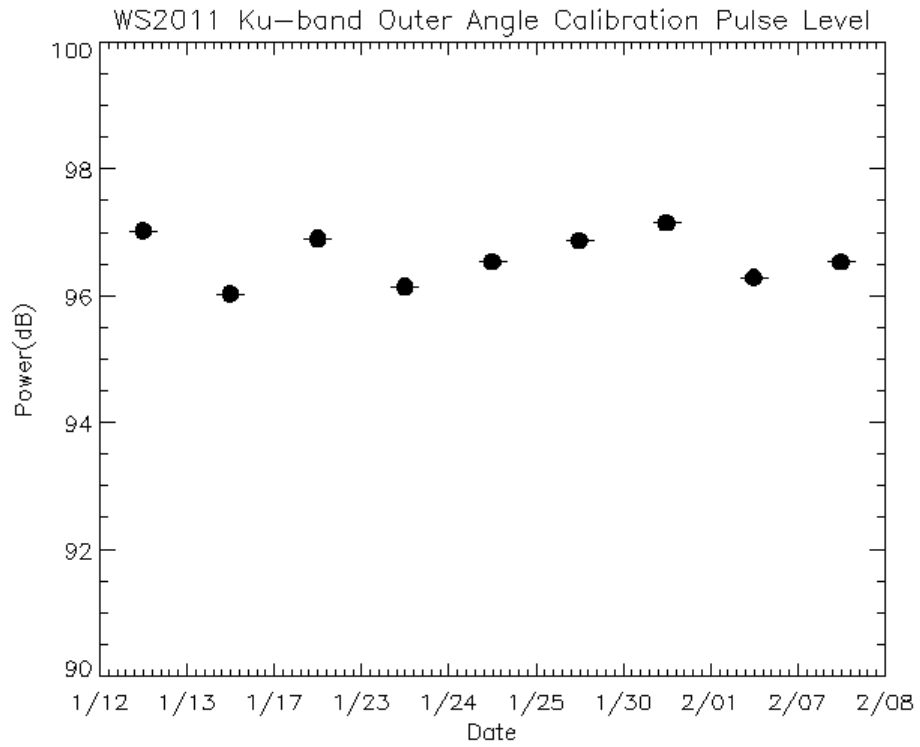


Figure 4.12: Ku-band Outer Angle Calibration Pulse Level for the 2011 winter season. The points represent the average pulse during a flight and the '-' represent the uncertainty of the average. The uncertainty is very small(i.e. negligible).

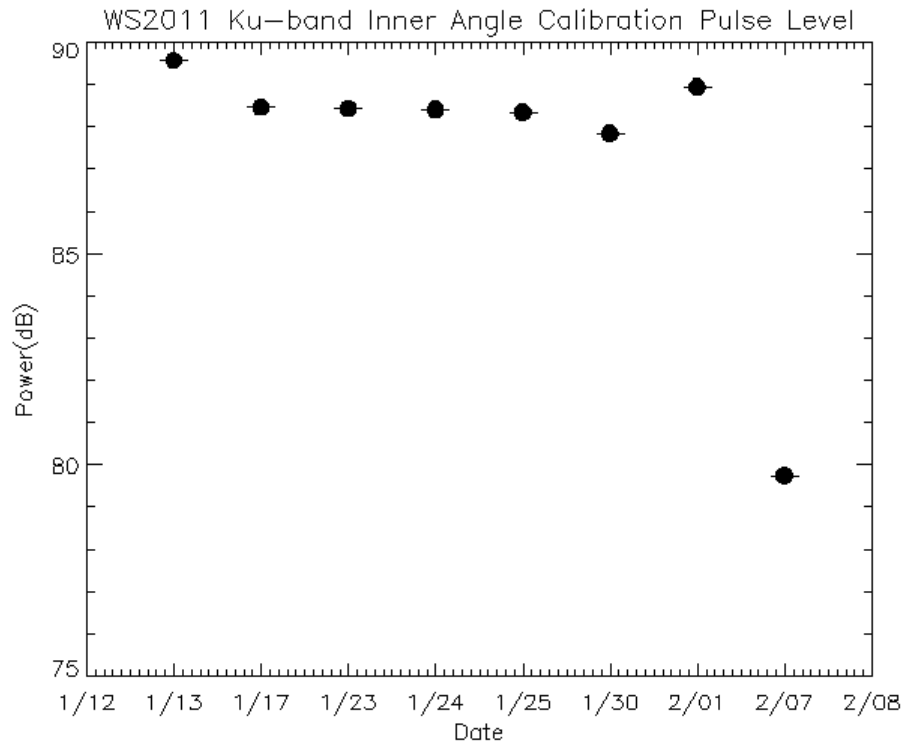


Figure 4.13: Ku-band Inner Angle Calibration Pulse Level for the 2011 winter season. The points represent the average pulse during a flight and the '-' represent the uncertainty of the average. The uncertainty is very small(i.e. negligible).

proves to be an accurate sample of the transmit pulse power. Though isolation issues were problematic during the past two seasons, when resolved the channels calibration pulse became stable within a reasonable deviation.

Table 4.1: The standard deviation of the calibration pulse over the course of a season. The table includes all four channels for the HS2010 and WS2011 season.

| Standard Deviation of Calibration Pulse | | | | |
|---|---------------|---------------|--------------|--------------|
| | Ku-band Inner | Ku-band Outer | C-band Inner | C-band Outer |
| HS2010 | 10.245 | 0.3775 | 0.742 | 2.4092 |
| WS2011 | 0.545 | 0.4016 | 3.091 | 4.6414 |

4.2 Encoder Signal Uncertainty

IWRAP employs a shaft encoder that records the angular position of the antennas and encodes them with a value between 0-4095. This digital data is sampled in parallel by a digital I/O card on a computer. This computer (known as “bigother”) samples the encoder data, adds a time stamp, and broadcasts it over a gigabit network to be merged with the rest of the data. The data acquisition computers receive this information over the network and merge it with the radar data.

It seemed as if the encoder number occasionally jumps by a few hundred points. Since this is not physically possible for the antenna to do, the problem must be with the way the data is being saved. This problem could not be recreated by saving encoder data directly to the computer but could still be seen in the encoder data that was merged with the rest of the data stream. In addition to this, the problem was only observed when plotting the encoder value versus consecutive packets. It disappeared when the encoder value was plotted versus time. This can be seen in Figure 5.12. This pointed to the problem actually laying with Pentek data acquisition card instead of the encoder acquisition. Additionally, radar data being saved also occasionally had drop outs.

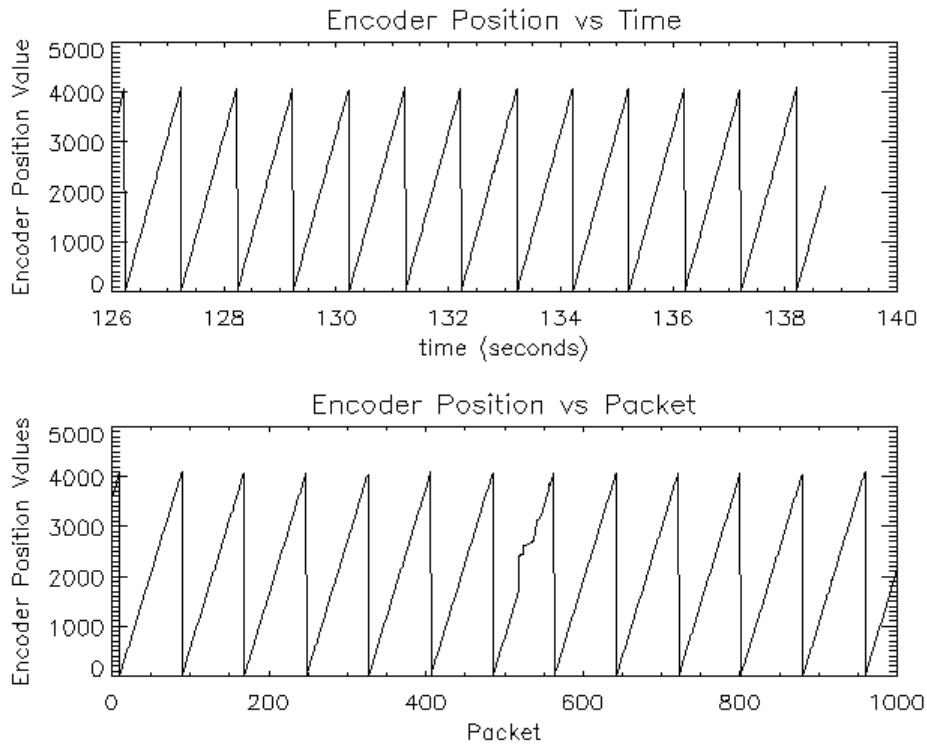


Figure 4.14: The top plot shows the encoder position versus time from data taken during the 2010 hurricane season. The bottom plot shows the same encoder data versus data packets. Note that the drastic jump in encoder value does not appear when plotted versus time.

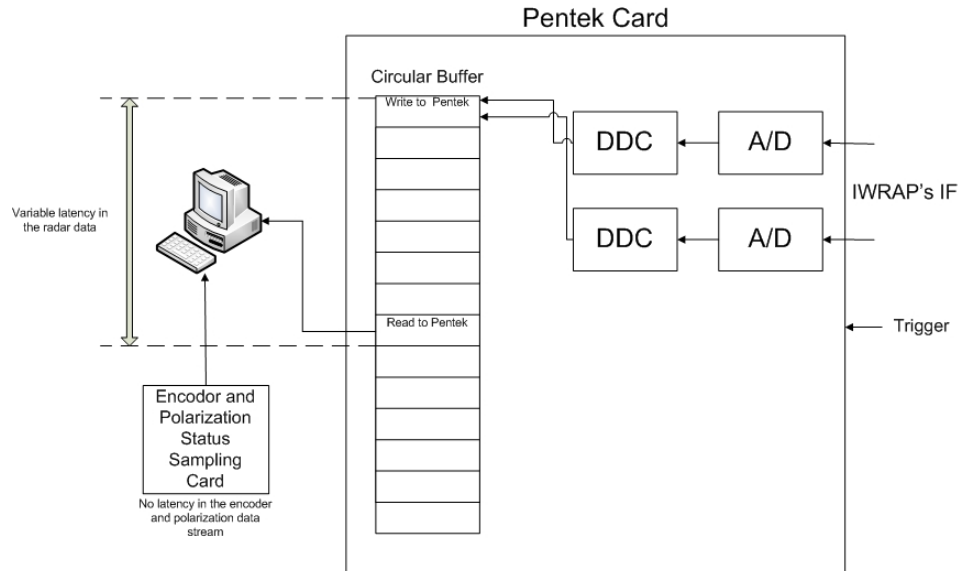


Figure 4.15: Diagram illustrating the flow of the data stream inside the Pentek digital receiver.

It was determined that this problem was the result of reading data of incorrectly merging the different data streams. The Pentek cards are given a trigger signal which is used to indicate when to read I and Q data from a circular buffer on the card. The I and Q data along with the rest of the data stream is compiled into a packet and saved to disk. If this does not happen fast enough then a trigger will be missed. If this happens, then the old I and Q data that was to be read during the missed trigger will be compiled into the current data stream. If enough triggers are missed then the unread data will be replaced with new data on the circular buffer. This is not as much of a problem if there is a small difference between the radar data and the rest of the data stream but if the difference becomes large enough the encoder data will no longer be useful. The circle buffer size was reduced so that the time lag would never be too large. The buffer is now only large enough to allow data for four triggers to be missed before an overrun occurs. This means that some data will occasionally go unread but the time lag between data streams will never be larger than one millisecond.

CHAPTER 5

CONCLUSION

5.1 Summary of Work Completed

This thesis has described the system improvements made to IWRAP from 2010 to 2011. The addition of dual-polarization capability added more value to IWRAP's data. This was done by adding new polarization switching and slip ring as well as altering the control signaling and data acquisition system to allow for this. Measurements taken at large incidence angles were discussed using two different methods. An up-to-date hardware description has been provided as well as a block diagram detailing the IF and RF electronics (in Appendix A). These are to be part of an IWRAP technical manual that will give future IWRAP users a current view of the system. Providing this as a separate document allows for easy integration with the rest of the manual. Different problems that were encountered during deployments are discussed with regard its effect on the data. Description of how these problems were solved is provided. This thesis also describes the quality of the data taken, after post processing, with these new hardware changes in place. The internal calibration of the system is analyzed showing that the system does a good job of sampling the transmitted power as long as proper isolation is provided between the transmit pulse and the calibration signal.

5.2 Future Work

After analyzing the stability of the system, steps should be taken to ensure a reliable calibration measurement. The leakage from the C-band power amplifier still

has a small effect on the calibration pulse. The C-band LNA should be relocated away from the power amplifier or it should be better shielded from the leakage. The Ku-band dual channel rotary joint has also caused issues of calibration signal instability. Moving the Ku-band front-end back to the other side of the rotary joint would ensure that this problem would not arise again. This would reduce the sensitivity of the Ku-band system but would provide a more reliable setup. An alternative to moving the Ku-band front-end is to ensure that the LNA has enough gain to overcome this leakage power. Other future work could be to add a trigger counter to the acquisition software to ensure that the radar data stream is synchronized with the rest of the data stream or to consider a new digital receiver configuration. Analysis of the dual-polarization and large incidence angle data is also needed. This data can be used to develop a GMF for the specifications that are being considered for the DFS.

APPENDIX

IWRAP TECHNICAL MANUAL ADDITIONS

A.1 RF and IF Electronics

The RF and IF section converts the 30 MHz signal to RF frequencies, then amplifies them before transmission. Upon reception, signals are routed through an LNA and down-convert to 30 MHz. In this description, the RF and IF component's model numbers will be given in parentheses. When two model numbers are given, the first corresponds to the C-band instrument, and the second one is for Ku-band. When only one model number is given, then the same component is used for both systems.

A.1.1 Reference Clock

A 10MHz oven controlled oscillator (Wenzel 501-04609A) is the reference clock to which all the frequencies of the radar are derived. This signal is provided to an IF board which splits the input and derives 30MHz, 40MHz, and 80MHz.

A.1.2 IF Transmit

The IF reference used for up and down-conversion is supplied by a Direct Digital Synthesizer (Analog Devices AD9858/PCBZ DDS). The DDS outputs the IF signal, which is either a 30MHz single tone or a linear frequency-modulated “chirp” centered at 30MHz. The DDS is controlled by an FPGA(Cyclone II DE-1 Development Board), and needs an input reference clock of 1 GHz (WV 9624-A02902). This DDS can store up to four different profiles enabling rapid (within 100 nsec) switching between the defined outputs, in the case of a chirp or a pulse. The DDS creates a frequency sweep by using a frequency accumulator, which regularly adds an incremental frequency to

the start frequency. This creates the frequency change that generates a chirp. The DDS needs 3.3 Volts, which is generated on the FPGA buffer Printed Circuit Board (PCB).

A.1.3 RF Transmit

There are two RF channels in each of IWRAP's radars. The first channel's RF is generated by a compact synthesizer (Herley-CTI XS-5315, Herley-CTI XS-1437) with a range of 4900 GHz to 5500 GHz for C-band and 12200 GHz to 13500 GHz for Ku-band. Channel two's RF signal is generated by a (Communication Techniques XPDRO-x.x46, Communication Techniques XPDRO-x.x216) oscillator. We have several of these which can be manually installed for different incidence angles. Both channels are sent through a isolator (Narda 4914, Narda 4916) then sent through power splitters (Narda 4314B-2, Narda 4316-2). One output of the splitters is sent to the receive-side for down-conversion, which is discussed later, while the other continues on the transmit path. The two transmit channels are sent through another isolator (Narda 4914, Narda 4916) and then a high-pass filter (Mini-Circuits SHP-1000) before both channels are sent into a S4DT switch.

The correct frequency is selected by the input ports of a SP4T switch (Narda SP143DHS) that rejects the other ports more than 60 dB. Since IWRAP no longer has four channels two of the SP4T switch powers are attached to matched loads. The signal is then sent through a single sideband mixer (Miteq SSZ0016, Stellex M38UC-30) where it is mixed with the RF signal to obtain the transmitted waveform. These mixers obtain the lower side band, so the input RF is decreased by 30 MHz after mixing. Before the RF signal reaches amplification stage it passes through a RF transmit switch (AMC SW2184-1a) so that no signal or noise is sent to be amplified when the system is receiving. In the Ku-band system, the signal is sent through a

pre-amplifier (MPN4-06001800-20P0) before being sent to the power amplifier. At this point, the RF is sent out of the transceiver to the front-end ready to be amplified.

The Ku-band front-end is mounted to the antenna assembly as opposed to being in the airplane cabin in a rack mount, as the C-band front is. This was done to reduce the amount of loss that the returned Ku-band signal experienced before reaching the LNA. Doing so gives an overall boost to the Ku-bands signal to noise ratio.

The RF power amplifiers are used to boost the power before it is transmitted. For C-band, a solid state amplifier (MA-Ltd AM50-5-5.5-48-48) with a 1dB compression point of +48dBm (63W) is used. For Ku-band, a transmitting wave tube amplifier (CPI VZM-63993J1) that applies a minimum of 32 dB of gain is used. Before being transmitted, the signal is coupled to the receiver through a coupler (KDI CA-752, KDI CA-872) for calibration purposes. The coupled signal is sent to the receiver chain which is described below. The through-port of the coupler is sent through an isolation switch (ENON ES0012, Hill Engineering 02WL0-M25-013) that provides extra isolation from the transmitter for the receive side. Then the signal is fed to a SP2T switch (Hill Engineering M24-005, Hill Engineering M25-002) that will switch between transmission and reception. Both switches have been designed to handle the peak power of the RF power amplifier. Cold switching (no RF signal applied) is required for the SP2T switch in order to not damage it. This signal is then sent out of the front-end box down to a rotary joint (Kevlin Microwave 1102, Kevlin dual channel rotary joint). Finally the RF signal is sent to a SP2T high power polarization switch (ENON ES0012, ENON ES0013), which is in charge of sending the signal to the proper polarization array.

A.1.4 Receiver

On the receiver side, a SP2T switch(Narda SP123DHS, AMC SWN-218-2DR) is selects between the received signal from the antenna and the measurement of the

transmitted signal from the calibration loop. For C-band, the signal is sent through a notch filter (Lorch Microwave 4BR4-5366/12-S) that is placed prior to the LNA to reject any signal coming from the lower fuselage radar (LFR) installed in the belly of the NOAA WP-3D aircraft. The LFR transmits a 6 microsecond pulse centered at 5.366 GHz, with a peak transmit power of 60 KW and a max antenna rotation speed of 4 rpm. IWRAP's received signal is amplified by an LNA (Miteq AMF-3S-4957-15, Miteq AFS4-02001800-35-ULN) then sent to the transceiver for down conversion. Since two incidence angles are transmitted for each PRF, during reception the two angles are down-converted simultaneously and independently. A four-way splitter (Narda 4314B-4, Narda 4316-4) is placed after the LNA. The outputs from the splitter are sent into two separate down-converter stages, one for each channel. The splitter is a remnant of when IWRAP had four channels for different four incidence angles. Two of the ports are terminated using matched loads. The channel generated using the RF oscillator has a very sharp cavity filter (Lark Engineering 6Cxxxx-75-4AA, Lorch Microwave 5CF7-xxxxx/250-S) which has a 75MHz bandwidth centered at the transmitted frequency providing a rejecting better than 30dB to the adjacent channel. The other channel that is generated by the RF synthesizer does not have such a filter since it will be set to provide different frequencies during a flight. The signals are then mixed down from RF using a single sideband mixer (Marki Microwave M01140, Marki Microwave M01082) which converts back down to a 30 MHz signal. A single sideband mixer was used to increase the rejection to the image frequency as well as reduce the system noise. The two signals are then sent into an IF amplifier (Mini Circuits ZKL-1R5). The signals are then sent through some attenuators to adjust the final signal so as not to exceed the power tolerance of the Pentek digital receiver cards. The signal is then fed into the two channel sampling card (Pentek 7131) where the signal is sampled and converted to baseband in which case it will be saved to disk.

Figure A.1 and Figure A.2 are the block diagrams of the RF and IF components of C-band and Ku-band, respectively.

A.2 IWRAP Instrument Control and Data Acquisition

A.2.1 Instrument Control

The control system consists of an Altera Cyclone II Field-Programmable Gate Array (FPGA) Development Kit and two buffer boards designed to convert the low-voltage TTL outputs of the FPGA to the 5V TTL required by the radar switches and digital receiver. The FPGA is programmed and controlled by the host computer, named “Beauty”. Using a 40MHz reference clock input, the Cyclone II creates all signals and triggers needed to control the radar. Also generated by the FPGA is the signaling required to program the Direct Digital Synthesizer (DDS). Figure A.3 is a picture of the box that houses these components.

The FPGA software takes inputs from IWRAP Graphical User Interface (GUI) and calculates wait-states, which correspond to pulse-widths, delays, and triggers. The FPGA employs a RS-232 serial input from a C program on Beauty, which sends data to be divided by a UART block into 8-bit packets. These packets are passed through each block, and eventually create the output control signals, DDS inputs, timing delays, and triggers required to run the radar.

To enable the switching controls output by the FPGA to work with the IWRAP switches and Pentek triggers, the signals need to be pulled-up from low-voltage TTL(3.3 volts) to 5 volts. The signals need to be split as the FPGA creates only one signal for each switch, and since both radars run simultaneously there needs to be a similar signal for each subsystem. The signals are split prior to being buffered, so as to not limit the current that each signal delivers. This buffer board also holds the voltage regulators used to create supply voltages for the DDS and FPGA. The FPGA needs an input voltage of 7.5 Volts, so a 15 Volt to 7.5 Volt regulator is used. The DDS needs 3.3 volts supply, so a 5 Volt to 3.3 Volt regulator is used. A PCB was

created to complete these functions. It houses three pull-up buffer chips, takes the FPGA signals as inputs and outputs the signals via a 50-pin header connector. The STMicroelectronics 74ACT244B buffer chip was chosen for its high-speed buffering, typically 4.6 ns. These chips are able to pull-up the voltage of its input signal up to its Vcc of 5.5 Volts. A second buffer board was created for the signaling that programs the internal synthesizers and the signal that indicates the current polarization state. Figures A.4 and A.5 show IWRAP's FPGA and buffer chips respectively.

A.2.2 Data Acquisition

IWRAP has two data acquisition computers, named Fantasy and Desire, that each have a Pentek 7131 digital receiver PCI card installed. Each pentek card takes a 80 MHz input clock, two 30 MHz IF channels from the radar subsystem and a trigger. Fantasy takes the IF from the Ku-band subsystem while Desire takes IF from the C-band subsystem. The data acquisition computers digitize the IF data, perform the final conversion to baseband, demodulate I and Q data and then store all raw data to a RAID system. The data acquisition computers also perform pulse-pair processing on the radar data, which is sent via UDP to be viewed on the real-time display (RTD) software on Beauty. Beauty is the radar operators computer that is used for starting, stopping and viewing the current data output of the system. The pentek trigger tells the data acquisition software when it is time to read another block of radar data from of the Pentek card. While the system is running, each channel generates approximately 20 Mbs of data. Figure A.6 shows how the data acquisition system is connected with the rest of the system.

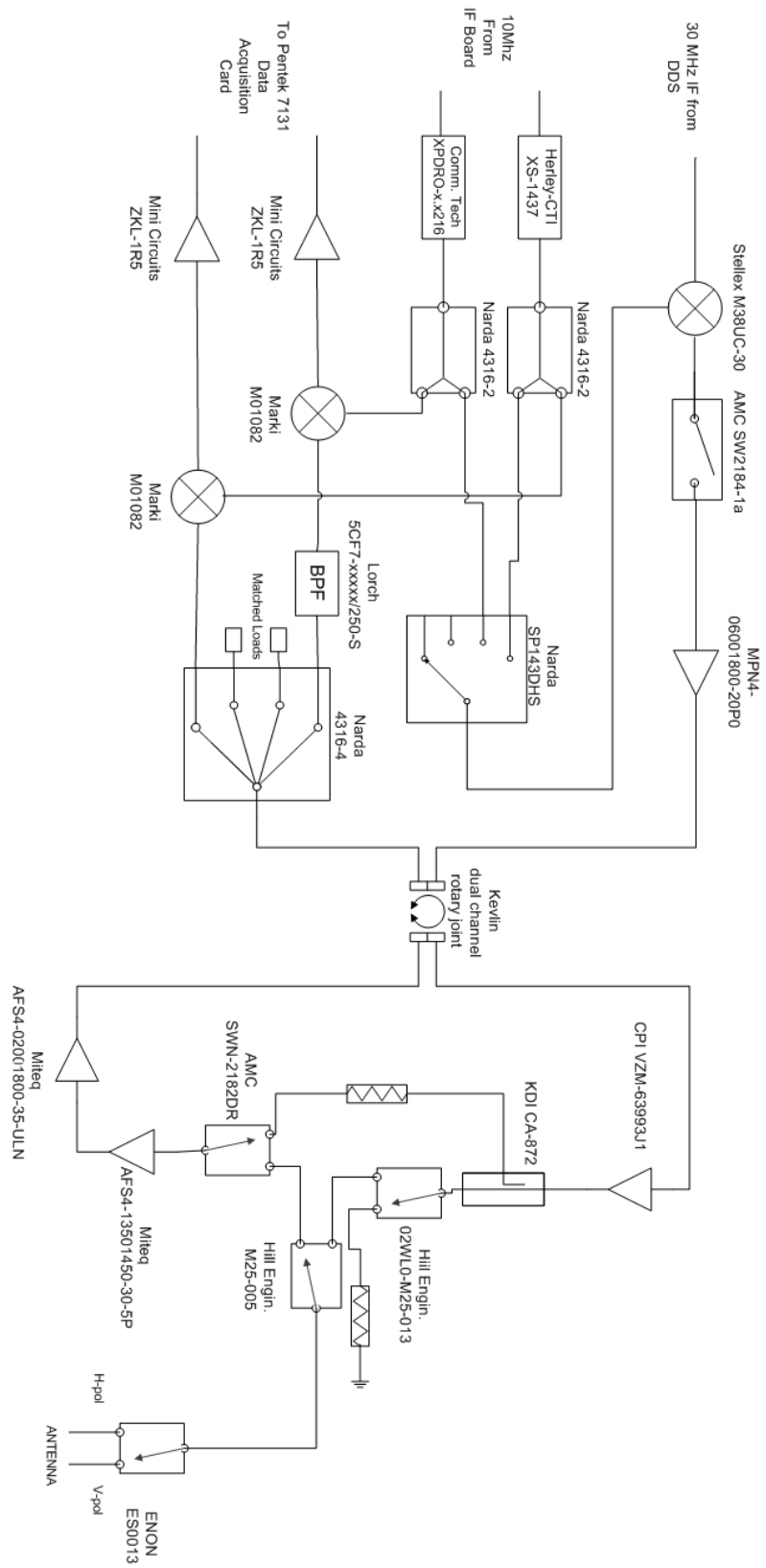


Figure A.2: Ku-band RF and IF block diagram

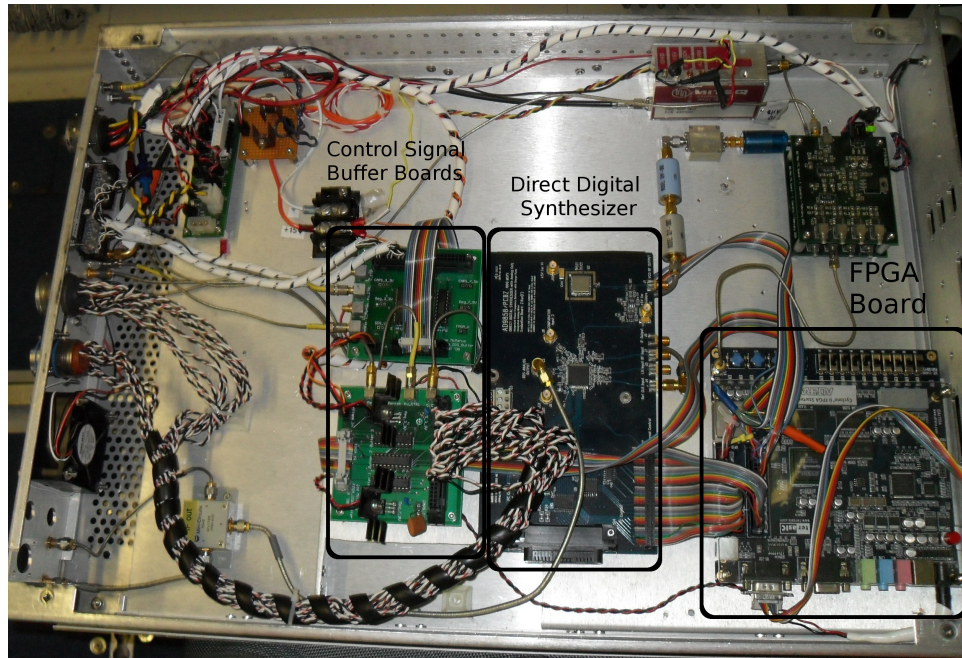


Figure A.3: Picture of the box that houses the FPGA, DDS, and buffer boards.

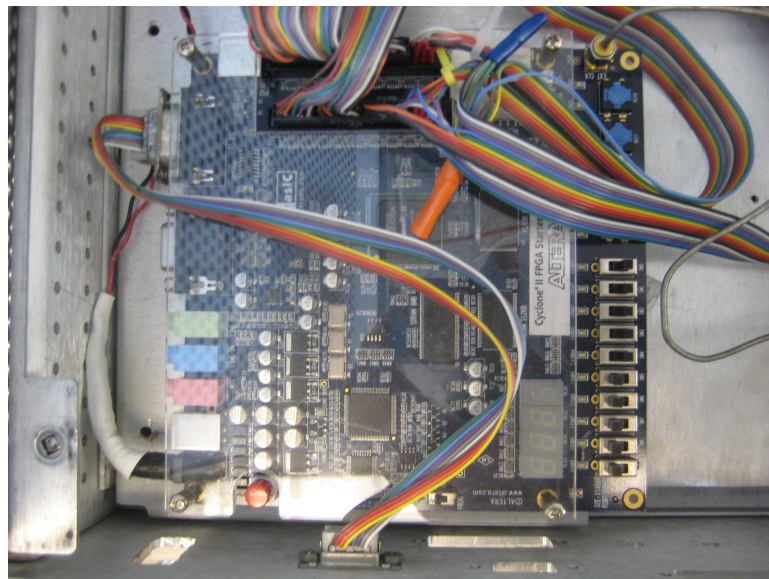


Figure A.4: IWRAP's Altera Cyclone II FPGA used to generate control signaling for the radar

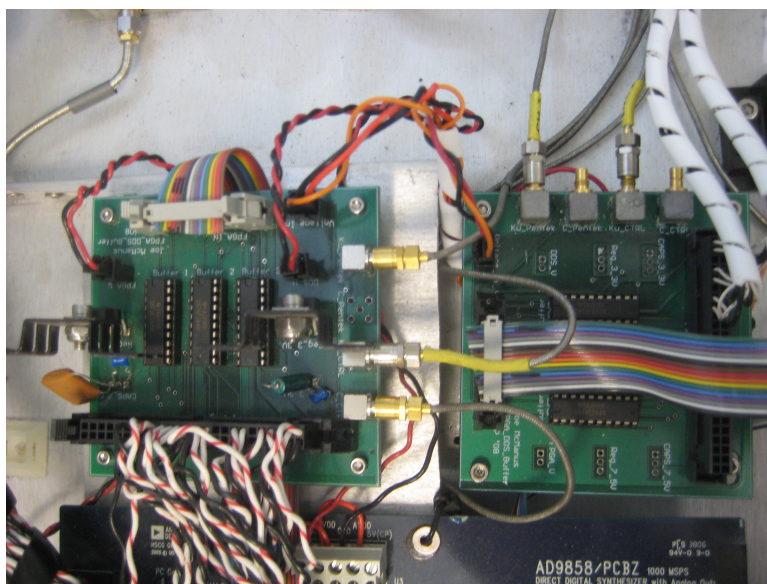


Figure A.5: IWRAP's buffer boards used to boost signaling from the FPGA to 5 volts

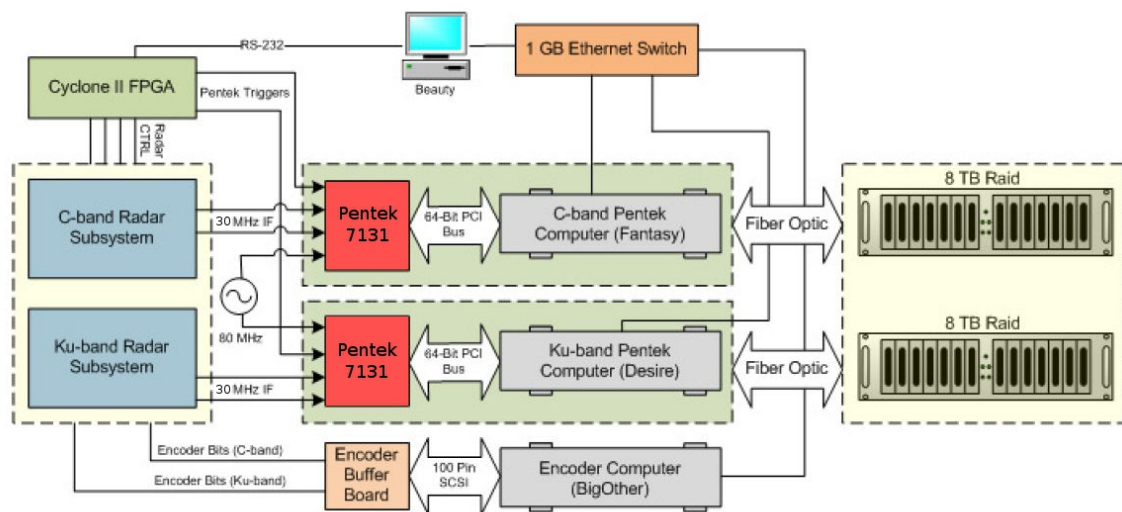


Figure A.6: A block diagram of IWRAP [10].

BIBLIOGRAPHY

- [1] Attema, E.P.W. The active microwave instrument on-board the ers-1 satellite. *Proceedings of the IEEE* 79, 6 (1991), 791–799.
- [2] Chu, Tao. Operation and improvement of the iwrap airborne doppler radar/scatterometer. *Masters thesis University of Massachusetts at Amherst* (2008).
- [3] Elachi, Charles, and ZYL, Jakob Van. Introduction to the physics and techniques of remote sensing. Jin Au Kong, Ed., John Wiley and Son, Inc., p. 373.
- [4] Falcon, Peter. Applications: Observing oceans from space. In *Available: <http://winds.jpl.nasa.gov/aboutScat/applications.cfm>*, [Accessed: April 30 2010].
- [5] Falcon, Peter. A history of scatterometry. In *<http://winds.jpl.nasa.gov/aboutScat/history.cfm>*, [Accessed: April 30 2010].
- [6] Frenandez, D. Esteban, Carswell, J. R., Frasier, S., Chang, P.S., Black, P. G., and Marks, F. D. Dual-polarized c- and ku-band ocean backscatter response to hurricane-force winds. *Journal of Geophysical Research VOL. 111* (2006).
- [7] Jelenak, Z., and Chang, P.S. Impact of the dual-frequency scatterometer on noaa operations. *Geoscience and Remote Sensing Symposium (IGARSS), 2010 IEEE International* (2010), 1808–1811.
- [8] Jones, W. L., and Zec, J. Evaluation of rain effects on nscat wind retrievals. *Proc. Oceans 96* (September 1996), 23–26.
- [9] Liu, W. T. Progress in scatterometer application. *Journal of Oceanography* 58 (2002), 121–136.
- [10] McManus, John J. Implementing pulse compression in the iwrap airborne doppler radar/scatterometer. *Masters thesis University of Massachusetts at Amherst* (2008).
- [11] Naderi, F.M., Freilich, M.H., and Long, D.G. Spaceborne radar measurement of wind velocity over the ocean-an overview of the nscat scatterometer system. *Proceedings of the IEEE* 79, 6 (1991), 850–866.
- [12] Torrence, Mark. Seasat. In *<http://ilrs.gsfc.nasa.gov>*, [Accessed: May 2 2010].

- [13] Tsai, W.-T., Spencer, M., Wu, C., Winn, C., and Kellogg, K. Seawinds on quikscat: sensor description and mission overview. *Geoscience and Remote Sensing Symposium, 2000. Proceedings. IGARSS 2000. IEEE 2000 International 3* (2000), 1021–1023.
- [14] Zec, J., and Jones, W.L. Tropical cyclone geophysical model function for ocean surface wind retrievals from nasa scatterometer measurements at high wind speeds. *Geoscience and Remote Sensing Symposium, 1999. IGARSS '99 Proceedings. IEEE 1999 International 2* (1999), 1013–1016.